CASE FILE
COPY

CALCULATIONS OF UNSTEADY TURBULENT BOUNDARY LAYERS WITH FLOW REVERSAL

J. F. Nash and V. C. Patel

Prepared by
SYBUCON, INC.
Atlanta, Ga.
for Ames Research Center

1. Report No. NASA CR–2546	2. Government Accession No.	3. Recipient's Catalog No.	
4. Title and Subtitle "Calculations of Unsteady Turbulent Boundary Layers with Flow Reversal"		5. Report Date May 1975	
		6. Performing Organization Code	
7. Author(s) J.F. Nash and V.C. Patel		8. Performing Organization Report No.	
		10. Work Unit No.	
9. Performing Organization Name and Address Sybucon, Inc. 9 Perimeter Place, N.W. Atlanta, Georgia		11. Contract or Grant No. NAS 2-7724	
		13. Type of Report and Period Covered Contractor Report	
12. Sponsoring Agency Name and Address National Aeronautics & Space Administration Washington, D.C. 20546			
		14. Sponsoring Agency Code	

15. Supplementary Notes

16. Abstract

The paper reports the results of a series of computational experiments aimed at studying the characteristics of time-dependent turbulent boundary layers with embedded reversed-flow regions. A calculation method, developed earlier by the authors and their co-workers, was extended to boundary layers with reversed flows for this purpose.

The calculations were performed for an idealized family of external velocity distributions, and covered a range of degrees of unsteadiness. The results confirmed those of previous studies in demonstrating that the point of flow reversal is non-singular in a time-dependent boundary layer. However, a singularity was observed to develop downstream of reversal, under certain conditions, accompanied by the breakdown of the boundary-layer approximations. A tentative hypothesis is advanced in an attempt to predict the appearance of the singularity, and is shown to be consistent with the calculated results.

17. Key Words (Suggested by Author(s)) Boundary Layer Theory Turbulent Flow Unsteady Flow Fluid Mechanics		18. Distribution Statement UNCLASSIFIED-UNLIMITED STAR Category 34	
19. Security Classif. (of this report) UNCLASSIFIED	20. Security Classif. (of this page) UNCLASSIFIED	21. No. of Pages 46	22. Price* $3.75

CONTENTS

FOREWORD

This report was prepared under Contract NAS2-7724 by

Sybucon, Inc.
Scientific and Business Consultants
9 Perimeter Place, N.W. (Suite 960)
Atlanta, Georgia 30339

for the

United States Army Air Mobility
Research and Development Laboratory
Ames Directorate
Moffett Field, California 94035.

The contract was administered by the National Aeronautics and Space Administration, Ames Research Center. The Technical Monitor was Dr. Lawrence W. Carr.

SUMMARY

The paper reports the results of a series of computational experiments aimed at studying the characteristics of time-dependent turbulent boundary layers with embedded reversed-flow regions. A calculation method, developed earlier by the authors and their co-workers, was extended to boundary layers with reversed flows for this purpose.

The calculations were performed for an idealized family of external velocity distributions, and covered a range of degrees of unsteadiness. The results confirmed those of previous studies in demonstrating that the point of flow reversal is non-singular in a time-dependent boundary layer. However, a singularity was observed to develop downstream of reversal, under certain conditions, accompanied by the breakdown of the boundary-layer approximations. A tentative hypothesis is advanced in an attempt to predict the appearance of the singularity, and is shown to be consistent with the calculated results.

LIST OF SYMBOLS

A, A_m Imbalance between production and dissipation of turbulent kinetic energy (see Equation (12))

a_1, a_2 Empirical functions in the shear-stress model (Equation (7))

c Chord length of the plate, and length of the integration domain

f Some undefined function

j, n Integers appearing in Equation (15)

L Dissipation length

P_x, P_y Pressure-gradient parameters defined by Equation (19)

p Static pressure

q Resultant fluctuating velocity ($q^2 = u^2 + v^2 + w^2$)

s Height of the integration domain

t Time

U, V, W Ensemble average velocity components in the x- , y- , z-directions, respectively

u, v, w Fluctuating velocity components corresponding to U, V, W, respectively

x, y, z Cartesian coordinates fixed in the plate: x measured along the plate, y measured normal to it, and z measured laterally.

x_o, x_1 Parameters appearing in Equations (2, 3)

α Shear-stress gradient (see Equation (14))

Γ, Φ Parameters appearing in Equations (7, 9)

Δ Step length in the numerical method

δ Boundary-layer thickness

δ^* Displacement thickness $\left(\delta^* = \int_o^\infty \left(1 - \frac{U}{U_e}\right) dy \right)$

$\varkappa$	Constant in the Law of the Wall
ν	Kinematic viscosity
ρ	Density
τ	Shear stress
Ψ	Stream function $\left(\Psi = \int_{o}^{y} U dy\right)$
ω	Parameters controlling the degree of unsteadiness in the flow (see Equations (1, 2, 3))

Subscripts

c	Convection values
e	Value at the edge of the boundary layer
m	Value at the matching station
max, MAX	Maximum values
o	Values at $x = 0$ (except x_o, which see)
p	Penetration value
s	Stagnation value
w	Value at the wall

LIST OF FIGURES

LIST OF FIGURES (continued)

I. INTRODUCTION

Theoretical methods for calculating the development of turbulent boundary layers in incompressible, time-dependent flow have been under active cultivation for the last several years. The method of Patel and Nash[1] established the basic framework for two-dimensional flows, and this method was improved and extended to infinite-yawed-cylinder flow by Singleton and Nash[2]. The latter method was used as the basis of a series of numerical experiments, by Nash et al[3] to determine the effects of time-dependence on flow-reversal onset, and a modified form of the method has been used in a study of flow reversal on pitching airfoils by Scruggs et al[4]. Another application has been to a study of the dynamics of hurricanes by Patel and Nash[5].

The work done up till now has been confined to flows either in which flow reversal did not occur, or where the point of flow reversal was moving upstream and the calculations were terminated at the reversal point. Now, it is well-known that the point of flow reversal in an unsteady flow is not a singular point. Hence, at least for flows in which reversal is moving upstream[*], it is natural to try to calculate the development of the boundary layer through the point of reversal, secure in the knowledge that boundary-layer theory has an application to the flow in some region beyond that point. In order to do so it is necessary to adopt a calculation method in which the integration proceeds in the time-direction, so that the convection of information in the upstream direction (upstream, that is, relative to the flow at infinity) can be handled in a proper manner. Attempts to calculate reversed flows by means of forward-marching schemes(advancing in the space-direction) either fail completely because of an essential instability problem, or are forced into stability artificially by violating the momentum equation.

We have said that for a certain class of flows, the boundary-layer equations remain valid in some region downstream of the point of flow-reversal; but this does not mean that they apply throughout the whole of the flow.

---

[*] In flows where the reversal point is moving downstream the boundary-layer equations may break down ahead of reversal; such flows are not discussed herein.

Extensive work in the laminar case[6,7,8,9] has shown that a singularity exists in the solution, forming a barrier beyond which the calculations cannot be continued.

The major objectives of the present work were to search for the appearance of a singularity in a family of time-dependent turbulent boundary layers, and, if one could be found, to try to determine the circumstances necessary for its appearance. To a large extent this objective has been achieved. Another objective was to gain further general understanding of the development of unsteady turbulent boundary layer, and this, too, has been realized to a considerable extent.

II. NATURE OF THE FLOWS CONSIDERED

The present studies relate to incompressible time-dependent flow over a two-dimensional surface which is flat or of large radius. Orthogonal coordinates are erected on the surface, with y measured normal to it, and x measured along the surface from some origin where the boundary layer is already turbulent and of known properties. The region of the surface, of interest, extends from $x = 0$ to $x = c$, where c is some positive reference length.

The velocity at the outer edge of the boundary layer is assumed to vary in some prescribed manner with both x and time t. Specifically, it is assumed that

$$U_e = U_o, \quad \text{for } t \leq 0 \quad \text{and all } x \tag{1}$$

$$U_e = U_o \left(1 - \omega t x/c\right), \quad \text{for } t > 0, \quad 0 \leq x \leq x_o, \tag{2}$$

$$U_e = U_o \left\{1 - \omega t \left(x_1 - x\right)/c\right\}, \quad \text{for } t > 0, \quad x_o < x \leq x_1, \tag{3}$$

where U_o is some reference velocity and ω is a parameter with dimensions t^{-1} describing the degree of unsteadiness in the motion; quasi-steady conditions correspond to $\omega \to 0$. In all the flows considered, x_o and x_1 were chosen such that $0 < x_o < c$, and $x_1 \geq c$. The velocity distribution over the upstream part of the plate ("plate" is used as shorthand for the portion of the surface: $0 \leq x \leq c$) corresponds to Flow C of Reference 3.

For increasing positive times, an increasing retardation is applied to the flow on the forward part of the plate ($0 \leq x \leq x_o$) and a recovering acceleration to the flow on the downstream part of ($x_o \leq x \leq c$). At some instant of time the wall shear stress, τ_w, at a station close to x_o, falls to zero. This event represents incipient reversal of the flow in the immediate neighborhood of the surface. For larger values of t, an embedded region of reversed flow exists on the plate, with the extent of this region increasing with time. For a range of values of x_o and x_1 the region of reversed flow remains confined to the plate either indefinitely, or for some specified time interval from $t = 0$. The present calculations

3

cover a range of conditions which ensure closure of the reversed-flow region ahead of the station $x = c$; this stipulation is made so as to avoid the situation in which a downstream boundary condition would need to be imposed. In the flows considered, the boundary-layer development is completely defined by the initial conditions, along $x = 0$ and $t = 0$, by the specified external velocity distribution, and by the Reynolds number.

At a time $t = t_s$, where

$$t_s = c/(x_o \omega) , \tag{4}$$

the velocity, U_e, at the outer edge of the boundary layer reaches zero at $x = x_o$, indicating stagnation of the external flow; the occurrence of this event forms a natural upper limit, to the range of t of interest, and all of the calculations were terminated at this point in time.

III.   THE CALCULATION METHOD

1.   Governing Equations

The velocity components in the x -, y -, z - directions are expressed in the form $U + u$, $V + v$, $W + w$, respectively, where U, V, W are defined as ensemble average velocities, with $w \equiv 0$ for a two-dimensional flow, and u, v, w are the residual fluctuating components about those ensemble averages. The governing equations are similar to those used in earlier studies [1,2,3], namely, the momentum equation:

$$\frac{DU}{Dt} + \frac{1}{\rho} \frac{\partial p}{\partial x} + \frac{\partial}{\partial y} (\overline{uv}) = 0 \tag{5}$$

the continuity equation:

$$\frac{\partial U}{\partial x} + \frac{\partial V}{\partial y} = 0 \quad , \tag{6}$$

and the empirically-modified turbulent kinetic-energy equation:

$$\frac{D\overline{uv}}{Dt} + 2a_1 \left[|uv| \frac{\partial U}{\partial y} + \Phi + \frac{\partial}{\partial y} (a_2 \overline{uv}) + \frac{\overline{uv}}{L} |uv|^{\frac{1}{2}} \right] = 0. \tag{7}$$

In Equations (5, 7) the convective derivative is defined by

$$\frac{D}{Dt} = \frac{\partial}{\partial t} + U \frac{\partial}{\partial x} + V \frac{\partial}{\partial y} . \tag{8}$$

In Equation (7) the empirical convective constant, a_1, and the empirical functions of position through the boundary layer, a_2 and L, are taken to be the same as those used in Reference 3; accordingly, the same cautionary statements apply to their continued use. Experimental substantiation of the appropriateness of Equation (7) and of the empirical parameters in it — or

5

guidance as to how they should be modified or improved — are still urgently needed and awaited. The quantity Φ in Equation (7) is the two-dimensional equivalent of the functions Φ_x, Φ_z in Reference 10, and is defined by

$$\Phi = \Gamma \left\{ |\overline{uv}| \frac{\partial U}{\partial y} + \overline{uv} \left|\frac{\partial U}{\partial y}\right| \right\} , \tag{9}$$

where Γ is some large number. The inclusion of this term has no effect on the resultant shear stress, but serves to maintain directionality of the shear-stress vector according to

$$\overline{uv} = a_1 \overline{q^2} \, \mathrm{sgn}\left(\frac{\partial U}{\partial y}\right) , \tag{10}$$

where $\overline{q^2}$ is the resultant mean-square velocity fluctuation. Equation (10) expresses an assumption which is implied in all the two-dimensional applications of Townsend's structural similarity hypothesis (see Ref. 10), on which the present model is based.

2. Solution of the Equations

The solution of the governing equations follows the approach of Reference 1, 2, 3. The flow is divided into an inner and an outer layer, with the matching station between them lying at about $y = 0.05\,\delta$. In the outer layer the equations are integrated by an explicit, staggered-mesh finite-difference scheme, advancing in the positive x-direction. The only aspect of the finite-difference scheme, worth mentioning here, concerns the method of obtaining x-derivatives. In order to avoid violation of the relevant zones of dependence, derivatives with respect to x are formed using two-point backward differences in region of positive U, and two-point forward differences in region of reversed flow (U < 0). At stations where the local flow direction is ambiguous: i.e. where the sign of U at some node point (x,y,t) is different from that at the adjacent points: $(x - \Delta x, y, t)$ __and__ $(x + \Delta x, y, t)$, the x-derivatives are set equal to zero. This refinement leads to improved smoothness of the solution at points of incipient flow reversal. Little loss of accuracy results because U, which

is multiplied by the x-derivative in the momentum equation, is inevitably close to zero at such points. It should be stressed that $\partial U/\partial x$ is not set equal to zero throughout the reversed-flow region, as has been done in certain other analyses of flows with reversal; such a procedure clearly leads to an invalid solution because typical values of $U\partial U/\partial x$ are by no means numerically small compared to the other terms in the momentum equation.

Further details of the numerical scheme, in the outer layer, can be found in Reference 2, 10, 11, 12, and the reader is referred thereto.

In the inner layer, near the surface of the plate, the numerical solution is again matched to an approximate solution based on the Law of the Wall. The details of this inner solution have been modified, as compared with the earlier work, in order to handle the transition from positive to negative values of the wall shear stress. In the present work, the turbulent kinetic-energy equation, for the inner layer, is written

$$\frac{\partial U}{\partial y} = \left\{ \frac{|\overline{uv}|^{\frac{1}{2}}}{\kappa y} + A(x,y,t) \right\} \, sgn \, (\overline{uv}) \, , \tag{11}$$

where the dissipation length, L, has been equated, in the usual way, to κy. The function A, where

$$A = \frac{1}{2a_1 \overline{uv}} \frac{D\overline{uv}}{Dt} + \frac{1}{\overline{uv}} \frac{\partial}{\partial y} (a_2 \overline{uv}) \, , \tag{12}$$

represents the residual imbalance between production and dissipation of turbulent kinetic energy which, near the wall, corresponds chiefly to convective transport. In the inner layer $A \ll |\partial U/\partial y|$, and is replaced by its value, A_m at the matching point with the outer-solution domain. With A_m now independent of y, we have, upon formal integration of Equation (11):

$$U = - \int_o^y \left\{ \frac{|\overline{uv}|^{\frac{1}{2}}}{\kappa y} + A_m \right\} \, sgn \, (\overline{uv}) dy. \tag{13}$$

The integral is evaluated, following Townsend[13], by prescribing a linear stress relationship

$$- \overline{uv} = \tau_w/\rho + \alpha y \, , \tag{14}$$

where α is independent of y, and typically of the same order as $\partial p/\partial x$. It is not difficult to perform the integration analytically; however the resulting forms: one, if $\overline{uv}$ is of the same sign throughout the inner layer, and two, if it changes sign, do not lend themselves readily to programming for the computer. To avoid these problems, Equation (13) is integrated by a simple iterative numerical scheme. With U and $\overline{uv}$ known at the matching point, an approximate value of τ_w is estimated from which α is determined; $\overline{uv}$ and U can then be found, as functions of y, for $0 < y < y_m$. The value of τ_w is adjusted, by means of a simple predictor-corrector method, until the associated values of U merge smoothly into those for the outer domain.

3. Integration Domain

The integration domain extended from $x = 0$ to $x = c$, and from $y = 0$ to $y = s(x)$ where $s = 1.25\ \delta$, approximately. The collocation points in the y-direction, 20 in number, were distributed, as in Reference 11, to give increased density near the wall. The collocation points in the x-direction were also distributed nonuniformly, so as to give increased density in the center portion of the plate. Specifically, the 24 points were distributed according to

$$x_j = 1.5\ \frac{j}{n} \left\{ 1 - \frac{j}{n} + \frac{2}{3} \left(\frac{j}{n}\right)^2 \right\} \, , \tag{15}$$

with $n = 24$ and $0 \le j \le n$.

4. Boundary Conditions

For times $t \le 0$, the flow corresponds to steady, constant-pressure flow in the x-direction. The boundary layer is in constant-pressure equilibrium, with a thickness, δ, at $x = 0$, of 0.00444 c. The Reynolds number: $U_o c/\nu$, is taken to be 10^7.

At $x = 0$, the velocity and shear-stress profiles are maintained, for all time, in the same form as at $t = 0$; i.e., in steady constant-pressure equilibrium with an external velocity of U_o and the Reynolds-number conditions specified above.

IV.   COMPUTATIONAL EXPERIMENTS

Two sets of computational experiments were conducted: designated Series A and Series B.   In Series A, the values

$$x_o = 0.5c \qquad (16)$$

$$x_1 = c$$

were used, yielding a symmetrical external velocity distribution, with U_e recovering to U_o at $x = c$. A range of $c\omega/U_o$ from 1 to 10 was covered. Analysis of the results from this first series, described in detail below, suggested that x_o and x_1 could profitably be increased — to improve resolution of the most interesting part of the flow without increasing computation times by adding more x-stations — and that the calculations should be extended to smaller values of $c\omega/U_o$. A second series: Series B, was then conducted, with x_o and x_1 increased in the ratio of 0.7; 1., i.e., with

$$x_o = 0.714c \qquad (17)$$

$$x_1 = 1.429c$$

and values of $c\omega/U_o$ down to 0.175 were considered.

The external velocity distributions corresponding to Series A and B are illustrated in Figure 1.

1. Series A

Distributions of wall shear and displacements thickness, from the calculations in Series A, are shown in Figures 2,3.   These results are for $c\omega/U_o = 10$, and the data are plotted versus longitudinal position on the plate, for discrete time levels up to $t = t_s$ (with $t_s = 0.2\, c/U_o$). The negative values of τ_w in Figure 2 indicate reversed flow near the wall. Incipient reversal occurs (for this value of ω) at about $t = 0.7t_s$, and, as t increases further, the region of reversed flow increases in extent.

10

The transition from positive to negative values of τ_w, and back again, is seen to be smooth — almost uneventful for the flow — and the variation of displacement thickness (Figure 3) is continuous in the vicinity of this transition. The displacement thickness increases to a maximum at some station between the point of flow reversal and the point of reattachment[*], and this maximum extends to infinity as $t \to t_s$ because of the vanishing of U_e. At $t = t_s$ the flow near the outer edge of the boundary layer becomes singular at $x = x_o$; however, velocity profiles close to x_o (discussed in connection with the Series B calculations, below) indicate that the flow over the greater part of the boundary-layer thickness does not break down, even at this point. In particular, τ_w appears to remain continuous through $x = x_o$ as $t \to t_s$, as is noted in Figure 2 and subsequent figures throughout this report. As noted earlier, the external velocity distributions are symmetrical about $x = x_o$; (the point x_o is indicated by an arrow in Figures 2, 3 and subsequent figures). The results of Figures 2, 3 exhibits substantial symmetry of τ_w and δ^*, about x_o, also. This is a consequence of the relatively large value of ω at which these results were obtained. At large values of ω, the effects of time-dependence, represented by the time-derivative term in the momentum equation, are dominant. Under such conditions, the displacement thickness is well represented by a relation

$$U_e \delta^* = f(x)$$

$$= (U_e \delta^*)_{t=0} \tag{18}$$

corresponding to the "high-frequency approximation" of Reference 3. It will be seen that, if U_e is symmetrical about x_o, Equation (18) requires symmetry of δ^* also.

---

[*] The term "reattachment" is strictly inappropriate, for the same reason that "separation" is inappropriate for describing the phenomenon of flow reversal. It is used here in the absence of a more suitable term, but it should be interpreted as the complement of flow reversal, not the complement of separation.

As ω decreases, the effects of spacial diffusion in the boundary layer, represented by the spacial gradients in the momentum equation, become more important. One result of this development is the deterioration of the symmetry of the flow about x_o. Figures 4, 5 show the distributions of τ_w and δ^*, versus x, for a range of values of ω. Reduction of ω is seen to be associated with an upstream movement of both the reversal point and the reattachment point, and with a marked change in the shape of both distributions. In particular, for $c\omega/U_o = 1.0$, there is a substantial increase in the level of displacement thickness around x = 0.3c, and a corresponding forward movement of the point of minimum wall shear stress. Moreover, there is a significant change in the level if this minimum as $c\omega/U_o$ is decreased from 2.0 to 1.0.

The flow on the downstream region of the plate: $0.7 \leq x/c \leq 1.0$, is relatively uninteresting, and it was decided to eliminate the region from the integration domain in the calculations of Series B; the decision led to the changes in the values of x_o and x_1 mentioned above. Furthermore, the interesting development of the flow, around $c\omega/U_1 = 1$, indicated that Series B should concentrate on the smaller values of ω.

2. Series B

Distributions of τ_w and δ^*, versus x, from the calculations of Series B, are shown in Figures 6 through 11, for successively lower values of ω. These results confirm and extend the observations from Series A concerning the growing asymmetry of the reversed-flow region and its surrounding flow. For $c\omega/U_o = 0.7$ (Figures 6,7), the forward movement of the point of minimum wall shear stress is noticeable, and there is a marked "bulge" in the distribution of δ^* versus x near x = 0.6c, i.e. substantially forward of x_o (note that $x_o = 0.714c$, now). As $c\omega/U_o$ is reduced to 0.35 (Figures 8,9) these effects are greatly magnified. The point of minimum τ_w, at $t = t_s$ is now only a short distance downstream of the reversal point, resulting in a large gradient of τ_w with respect to x. There is also a large gradient in the corresponding distribution of the displacement thickness (Figure 9), and δ^* now has a second maximum near x = 0.4c. Downstream of these regions of large gradient there is some deterioration in the quality of the numerical solution as evidenced by the waviness of the τ_w - distributions in Figure 8; however the solution did not break down and

results could be obtained throughout the reversed-flow region and downstream of it.

At the lowest value of ω considered ($c\omega/U_0 = 0.175$), steep gradients in both τ_w and δ^* begin to occur, at times of around $0.65\ t_s$ (Figures 10, 11). the region of steep gradients, in each distribution, forms and then moves upstream, towards the point of flow reversal, with increasing time. Above a time of $0.85\ t_s$ the gradients become so large that the solution was found to break down aft of the region in question and it was not possible to obtain results downstream of about $0.4c$.

The development of regions of locally high gradient is further illustrated by Figures 12, 13, in which results are presented, for a range of values of ω, for time $t = t_s$. It is evident that a profound change in the character of the flow occurs between values of $c\omega/U_0$ of 0.7 and 0.35. Results for a value of 0.525 appear to be on the borderline.

In order to illustrate this change in flow character in more detail, Figures 14, 15 show a reconstruction of the physical features of the flow. Typical velocity profiles are plotted to scale, and the boundary of the reversed-flow region (the locus $U = 0$) is drawn. The results correspond to $t = t_s$, and the boundary $U = 0$ extends to the edge of the boundary layer locally at $x = x_0$. However, as remarked earlier, the vanishing of U_e causes no significant perturbation in the solution; δ^* becomes infinite at $x = x_0$ and $t \rightarrow t_s$, but the product $U_e \delta^*$ is found to remain continuous through $x = x_0$. Much more interesting than the development of the flow near $x = x_0$, is its development a short distance downstream of the point of reversal. The velocity profiles at $x = 0.484c$, shown in Figures 14, 15, indicate the large increase in the reversed-flow velocities, and the large increase in the thickness of the reversed-flow region, as $c\omega/U_0$ is reduced from 0.7 to 0.35. The overlapping of the profiles at $x = 0.266c$ and $0.484c$, as they are drawn in Figure 15, is indicative of the substantial increase on the velocity gradient; $\partial U/\partial x$, compared with the conditions shown in Figure 14.

The change in flow character is further illustrated by the instantaneous streamline patterns plotted in Figures 16, 17. These have been reconstructed to the extent possible from the calculated velocity profiles. For $c\omega/U_0 = 0.7$, Figure 16, the recirculatory flow has a fairly regular appearance, and the slope of the streamlines, just downstream of reversal is

not excessive (note the expanded y-scale in the figure). At $c\omega/U_o = 0.35$, however (Figure 17) the recirculatory flow has become grossly distorted, and also there is bunching of the streamlines, which have acquired a steep slope immediately downstream of reversal.

More detailed velocity profiles, for the two cases: $c\omega/U_o = 0.7$ and 0.35, are shown in Figures 18, 19. In each case, the transition from forward to reversed flow is smooth and continuous. However, the flow at the smaller value of ω is characteristized by large values of the derivative $\partial U/\partial x$, and by rapid expansion of both the boundary-layer thickness and the thickness of the reversed-flow region already noted.

The rapid increase in boundary-layer thickness, and the steepening of the gradients, observed for values of $c\omega/U_o$ below 0.35, causes doubts to be cast on the continuing validity of the boundary-layer approximations. It emerges that these doubts are well-founded. Figures 20, 21 present data on the normal pressure gradients implied by the solutions. It has to be stressed that the normal gradients have not been taken into account in the calculation; however they can be computed in retrospect, and their largeness would then indicate a serious inadequacy of the solution. Validity of the boundary-layer approximations requires that the change in pressure across the boundary layer be small enough that the assumption of constant $\partial p/\partial x$ remain realistic. Now, the change in pressure across the boundary layer is measured by a typical value of $\delta \partial p/\partial y$, the value at $y = \delta$, say. Accordingly, it is appropriate to compare the magnitudes of P_y and P_x, where

$$P_y = \frac{\delta}{\rho U_o^2} \left| \frac{\partial p}{\partial y} \right|_{y=\delta} \quad , \quad \left(\text{with } \frac{\partial p}{\partial y} \doteq U \frac{\partial V}{\partial x} + V \frac{\partial V}{\partial y} \right)$$

$$P_x = \frac{c}{\rho U_o^2} \frac{\partial p}{\partial x} ; \tag{19}$$

for the boundary layer approximations to be valid, P_y must be small compared to P_x. Figure 20 indicates that, for $c\omega/U_o = 0.7$, $P_y \ll P_x$ everywhere (except possibly at the point where P_x vanishes), and the boundary-layer approximations evidently remain intact. This is true even though the normal velocity, V, is not always small compared with U_o; even at $y = \delta$, local values of V/U exceed 0.4. At $c\omega/U_o = 0.35$, however,

14

(Figure 21) the normal pressure gradients, measured by the value of P_y, become large near $x = 0.4$ c; in fact $P_y > P_x$ at one station. This is ample evidence that the boundary-layer approximations are no longer valid in this region of the flow, and it will be observed that this region corresponds, approximately, to the region in which the gradients of τ_w and δ^* are large.

The observation that, for small values of ω, there occur regions within the flow in which steep gradients arise, accompanied by bunching and sharp deflection of the streamlines, and the breakdown of the boundary-layer approximations, leads convincingly to the conclusion that singular- or quasi-singular — behavior has been encountered in the solution. Because of the coarseness of the integration mesh it is not possible to isolate a mathematical singularity in either strength or position. However the rough location of the singularity is readily determinable. To return to Figures 11, 13, for example, there appears to be justification for using the simple criterion $\delta^*/c > 0.1$ to indicate the approximate point of initiation, and subsequent movement, of the singularity. No suggestion is being made that such a criterion has general applicability, but it seems to be appropriate here.

In the present context we are discussing only the position of the singularity in the x-t plane. It is less easy to determine the position in the y-direction, but it does not seem to occur at the point of maximum reversed-flow velocity, i.e., where $\partial U/\partial y = 0$, as suggested by Sears and Telionis[6]. Indeed Figure 19 shows that the maximum levels of $(-\partial U/\partial x)$, and hence also the maximum levels of $\partial V/\partial y$, occur much further from the wall. The difference in behavior between the present, turbulent case, and the laminar case studied by Sears and Telionis, is evidently associated with the difference in the relationship between the shear stress and the velocity gradient, $\partial U/\partial y$.

Figure 22 shows a plot of the locus of the singularity, for the two calculations where it was observed, compared with the loci of the reversal and reattachment points. The singularity appears to form within the region of x bracketed by these two points, and then to move upstream in pursuit, as it were, of the reversal point.

Also shown in Figure 22, for each value of ω, is an arrow

indicating the direction followed by a particle moving in the maximum negative velocity: $(-U)_{MAX}$, say, reached anywhere in the reversed flow region during the time interval $t \leq t_s$. At any particular time, the maximum negative velocity $(-U)_{max}$, say, occurs some distance downstream of the reversal point, and its value increases almost linearly with time (see Figure 24, below); $(-U)_{MAX}$ is the value of $(-U)_{max}$ corresponding to $t = t_s$. $(-U)_{MAX}$ increases with the reduction of ω; as $c\omega/U_o$ is reduced from 1.4 to 0.35, it increases by a factor of around 2.3. In contrast, the rate of forward movement of the point of flow reversal decreases with the reduction of ω ; in fact it varies approximately as $\omega\ f(x/c)$, over the range $0.175 \leq c\omega/U_o \leq 1.4$, a property which enables a "similarity" plot such as Figure 23 to be constructed. The rate of forward movement of the reversal point can conveniently be referred to as the penetration velocity, $(-U)_p$, signifying the penetration of the oncoming boundary layer by the reversed flow.

To return to Figure 22, it is interesting to note the relationship between the direction representing $(-U)_{MAX}$ and the slope of the reversal locus which represents the penetration velocity. At the higher values of ω , where there is no singularity, $(-U)_{MAX}$ is smaller than $(-U)_p$. At the low values of ω , however, where there is a singularity, $(-U)_{MAX}$ exceeds $(-U)_p$. This observation suggests that a more careful examination of the velocities in the reversed-flow region might yield useful insight into the conditions necessary for the development of the singularity.

Two possible lines of approach suggest themselves, in this regard: one involving the transport of mass in the reversed-flow region, and the other involving the convection of disturbances through the region. Both depend on the definition and evaluation of a characteristic convection velocity, $(-U)_c$, say, for the reversed-flow region. This convection velocity will evidently be lower than $(-U)_{max}$, but will be related to it. The argument involving mass transport focusses attention on the rapid increase of the thickness of the reversed-flow region which occurs in the neighborhood of the singularity (see Figure 15), and on the corresponding displacement of the streamlines away from the wall (Figure 17). This combination of events can take place only if there is a net inflow of fluid, into the portion of the boundary layer in question, by way of convection in

16

the negative x-direction. The section of boundary layer is bounded, on the upstream side by the reversal point which is traveling at the penetration velocity, $(-U)_p$. Accordingly, the necessary mass inflow requires that the convection velocity, $(-U)_c$, which characterizes the rate of mass transport from downstream, must be greater than $(-U)_p$. If it is less than $(-U)_p$, then mass will not enter the region, and the build-up of fluid accompanying the development of this singularity, will not occur.

The argument involving the convection of disturbances regards the singularity as having some of the characteristics of a shock wave. According to this argument the singularity can exist only if disturbances are being convected towards the singularity. Hence, paying attention to signs, we must require the convection velocity, as measured by an observer traveling with the singularity, to be negative. It is evident, from Figure 22, that after its inception the singularity moves at about the same velocity as the reversal point, or, in other words, at the penetration velocity, $(-U)_p$. Thus, finally, we require that the convection velocity $(-U)_c$, must be greater than the penetration velocity for a singularity to be established, which results in the same criterion as before.

The tentative hypothesis thus emerges that a singularity will form if, and only if, $(-U)_c > (-U)_p$. In order to test the validity of this hypothesis some value has to be attached to the convection velocity $(-U)_c$. Here, for simplicity, a value of $\frac{1}{2}(-U)_{max}$ is used. The variation of this velocity with time, for a range of ω, is shown in Figure 24, and the penetration velocity, $(-U)_p$, is plotted for comparison. According to the hypothesis, the point of intersection of the curves representing $(-U)_c$ and $(-U)_p$ corresponds to the point of inception of the singularity, and an inception boundary, so defined, is plotted in Figure 25, as a function of ω and time. The region below and to the left of the boundary represents the domain of non-singular flow, while the region above and to the right of the boundary represents the domain of singular flow. The boundary crosses the curve defined by $t = t_s$, indicating that a singularity should be expected to appear, sometime during the motion, for values of $c\omega/U_o$ less than about 0.6.

The actual points of inception of the singularity, taken from the calculations of $c\omega/U_o = 0.175$ and 0.35, plot as points just inside the domain of singular flow indicated by Figure 25; these results accordingly

lend support to the correctness of the hypothesis. The point corresponding to $t = t_s$ and $c\omega/U_o = 0.7$ lies just inside the domain of _non-singular_ flow, and the apparent absence of a singularity in that calculation provides further support. The point corresponding to $t = t_s$ and $c\omega/U_o = 0.525$ falls in the singular domain, indicating the likelihood of a singularity in the flow although none was observed in the calculation. This last result is thus at variance with the hypothesis. However, the calculation for $c\omega/U_o = 0.525$ was judged to be borderline, and the variance cannot be regarded as a serious one. Indeed it must be remembered that the precise location of the boundary drawn in Figure 25 depends on only a rough estimate of the appropriate value of the convection velocity, $(-U)_c$.

By and large, it could be claimed that the calculated results support the hypothesis, crude as it is, and the arguments underlying it. The singularity appears to have some of the characteristics of an explosive accumulation of fluid, which erupts out into the external stream. It also appears to have some of the characteristics of a shock wave, in the reversed-flow region, with the convection velocity playing the role of the supersonic component (U-a) of the flow approaching the shock. The analog between the two flows should not, however, be pushed too far; it is most unlikely, for instance, that the existence of the singularity in the present flow has anything to do with the hyperbolic nature of the governing equations. After all, its counterpart in laminar flow occurs in a setting where the equations are purely parabolic.

V. CONCLUSIONS AND RECOMMENDATIONS

The work described herein has demonstrated the feasibility of performing calculations for unsteady turbulent boundary layers with embedded reversed-flow regions, and has shed light on some of the basic properties of such flows.

The results confirm the statements made in earlier work (a) that the onset of flow reversal in a turbulent boundary layer, is delayed by the effects of time-dependence, and (b) that the point of flow reversal is not a singular point in a time-dependent boundary layer.

The present calculations were performed for a family of prescribed external velocity distributions in which the relative importance of the effects of time-dependence, compared to those of spacial diffusion, was controlled by a parameter ω . The external velocity distributions were designed to impose a retardation on the boundary layer, starting at $t = 0$, and progressing to the point in time, $t = t_s$, when stagnation of the external flow occurred at one longitudinal station. The distributions were chosen to produce a closed region of reversed flow: confined within the domain of the numerical solution, to avoid the necessity of furnishing a downstream boundary condition.

The results show that, for sufficient large values of ω , the calculation could be completed, up to $t = t_s$, before any breakdown of the boundary-layer approximations occurred, and before any singularity occurred in the solution. Over this range of conditions, corresponding to strong time-dependence, the reversed-flow region, and its surrounding flow, exhibited only minor effects of spacial diffusion. At smaller values of ω , a singularity — or quasi-singularity — was observed to form: at a time later than that for incipient reversal and at a longitudinal position between the reversal point and the end of the reversed-flow region. The inception of this singularity was characterized by steepening longitudinal gradients, sharp deflection of the streamlines away from the surface, and the local breakdown of the boundary-layer equations. The singularity was observed to form and then to move upstream towards the reversal point, eventually maintaining a roughly constant distance from it.

The conditions necessary for appearance of a singularity appear to involve the existence of an appropriate relationship between the dominant

velocities in the reversed-flow region and the rate of forward movement of the reversed point. Two simple, heuristic arguments, one focussing on mass transport and the other focussing on the convection of disturbances, lead to the formulation of the same tentative hypothesis: that a singularity will exist in the flow if, and only if, the typical reversed-flow velocities exceed the rate of penetration of the reversed flow into the oncoming boundary layer. The results of the present calculations lend support to the correctness of this hypothesis.

The present calculations were restricted to a single family of external velocity distributions, and they should be extended to a wider range of distributions in order to generalize the results. One important question, which arises, is concerned with the effect of different downstream conditions on the appearance and location of the singularity. The existence of the reversed flow clearly provides a mechanism by which information can be transmitted upstream into the neighborhood of the reversal point. On the other hand, the rate of convection of this information — and the effect it is likely to have — would appear to involve considerations similar to those discussed in the context of the formation of the singularity. It is possible that similar considerations determine both the appearance of a singularity and the sensitivity to downstream conditions. This possibility needs to be explored.

Another important extension of the present work should be to external velocity distributions more typical of real aerodynamic situations. It should be noted that throughout the range of conditions in which no singularity exists, the boundary-layer approximations appear to remain valid. Accordingly, the computed displacement thicknesses can be used to perturb the external flow via some interactive model in which the boundary-layer and its environment are appropriately coupled. The applicability of such a model is restricted — not by the occurrence of flow reversal — but by the occurrence of a singularity. Useful ranges of conditions would appear to exist in which the interaction calculations can proceed even though reversed flow has already been established.

REFERENCES

1. V. C. Patel and J. F. Nash, "Some Solutions of the Unsteady Turbulent Boundary Layer Equations," _Recent Research on Unsteady Boundary Layers_ (Proc. I.U.T.A.M. Symposium, Quebec 1971), A.E. Eichelbrenner, ed., Presses de l'Université Laval, Quebec 1972.

2. R. E. Singleton and J. F. Nash, "A Method for Calculating Unsteady Turbulent Boundary Layers in Two-and-Three Dimensional Flows," _AIAA J._ 12, No. 5, May 1974.

3. J. F. Nash, L. W. Carr and R. E. Singleton, "Unsteady Turbulent Boundary Layers in Two-Dimensional Incompressible Flow," A.I.A.A. 6th Fluid & Plasma Dynamics Conf., Paper No. 73-650, July 1973, (to be published in the _A.I.A.A. Journal_).

4. R. M. Scruggs, J. F. Nash and R. E. Singleton, "Analysis of Flow-Reversal Delay for a Pitching Foil," A.I.A.A. 12th Aerospace Sciences Meeting, Paper No. 74-183, Feb. 1974.

5. V. C. Patel and J. F. Nash, "Numerical Study of the Hurricane Boundary-Layer Mean-Wind Profiles," Final Report, Contract 4-35831, Dept. of Commerce, June 1974.

6. Sears, W. R. and Telionis, D. P., "Unsteady Boundary-Layer Separation," Recent Research Boundary Layers (Proc. I.U.T.A.M. Symposium, Quebec 1971), E. A. Eichelbrenner, ed., Presses de L'Université Laval, Quebec 1972.

7. D. P. Telionis and M. J. Werle, "Boundary-Layer Separation from Downstream Moving Boundaries," _J. Appl. Mech._, p. 369, June 1973.

8. D. P. Telionis, D. Th. Tsahalis and M. J. Werle, "Numerical Investigation of Unsteady Boundary-Layer Separation," Virginia Pol. Institute and State University, Paper VPI-E-72-14, Sept. 1972.

9. D. P. Telionis and D. Th. Tsahalis, "The Response of Unsteady Boundary-Layer Separation to Impulsive Changes of Outer Flow," AIAA 6th Fluid and Plasma Dynamic Conf., Paper No. 73-684, July 1973.

10. J. F. Nash and V. C. Patel, "Three-Dimensional Turbulent Boundary Layer," _SBC Technical Books_, 1972.

11. J. F. Nash, "An Explicit Scheme for the Calculation of Three-Dimensional Turbulent Boundary Layers," _J. Basic Eng._, 94D, p. 131, March 1972.

12. J. F. Nash and V. C. Patel, "A Generalized Method for the Calculation of Three-Dimensional Turbulent Boundary Layers," Proc. Project SQUID Workshop, Ga. Inst. Tech., (Ed. J. F. Marshall), June 1971.

13. A. A. Townsend, "Equilibrium Layers and Wall Turbulence," _J. Fluid Mech._, p. 97, 1961.
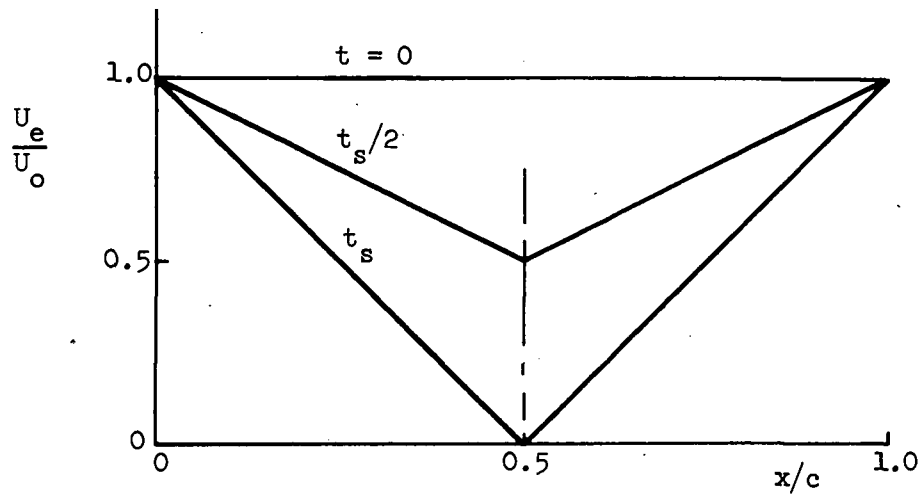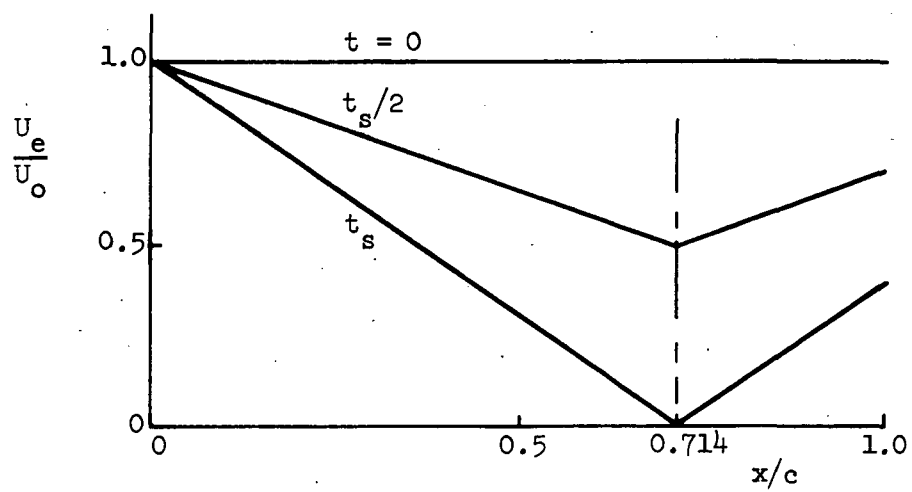
Figure 1. External Velocity Distributions
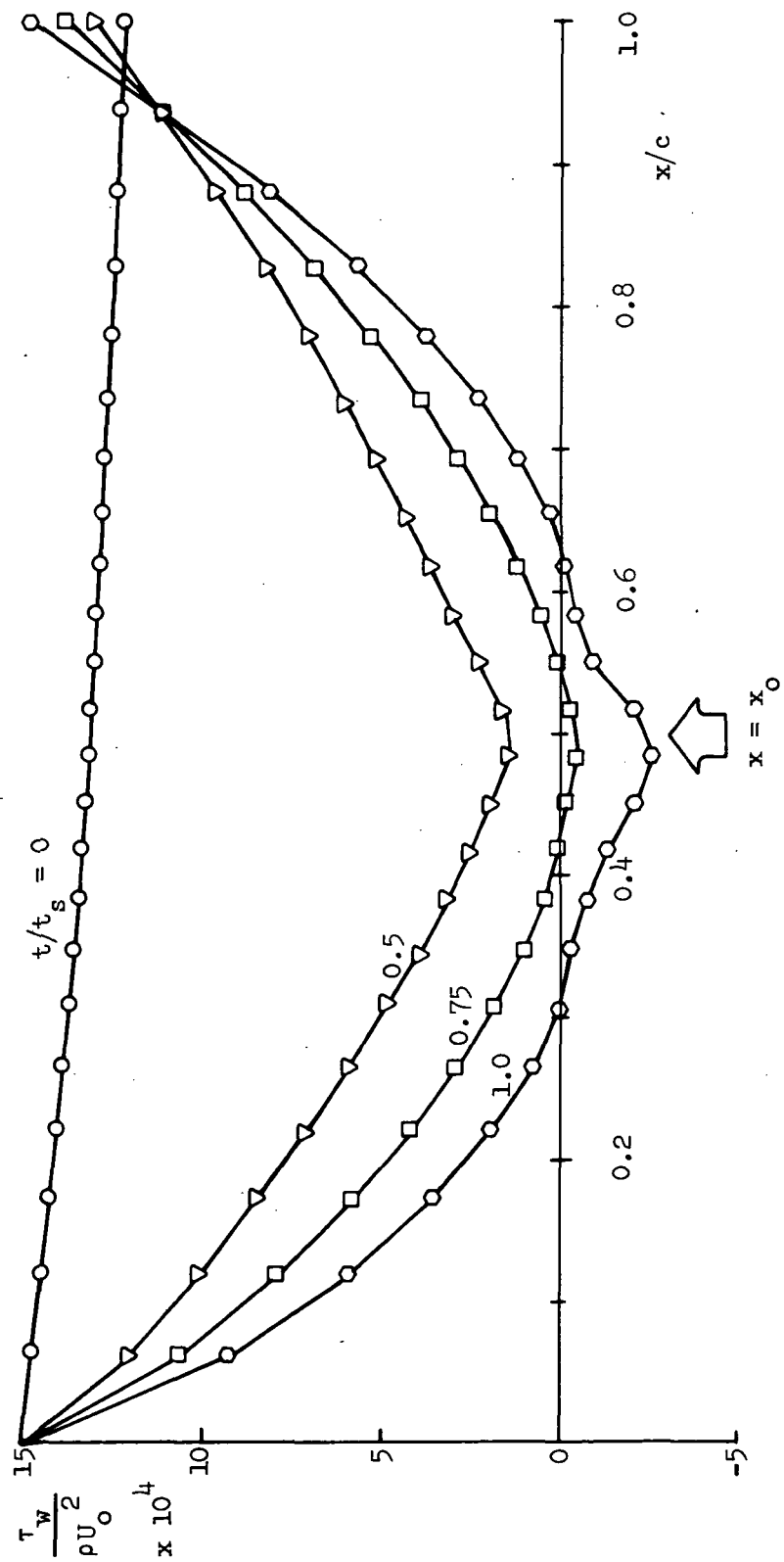
Figure 2. Wall Shear Stress Distributions for Increasing Time $\left(c\omega/U_o = 10 \right)$

23
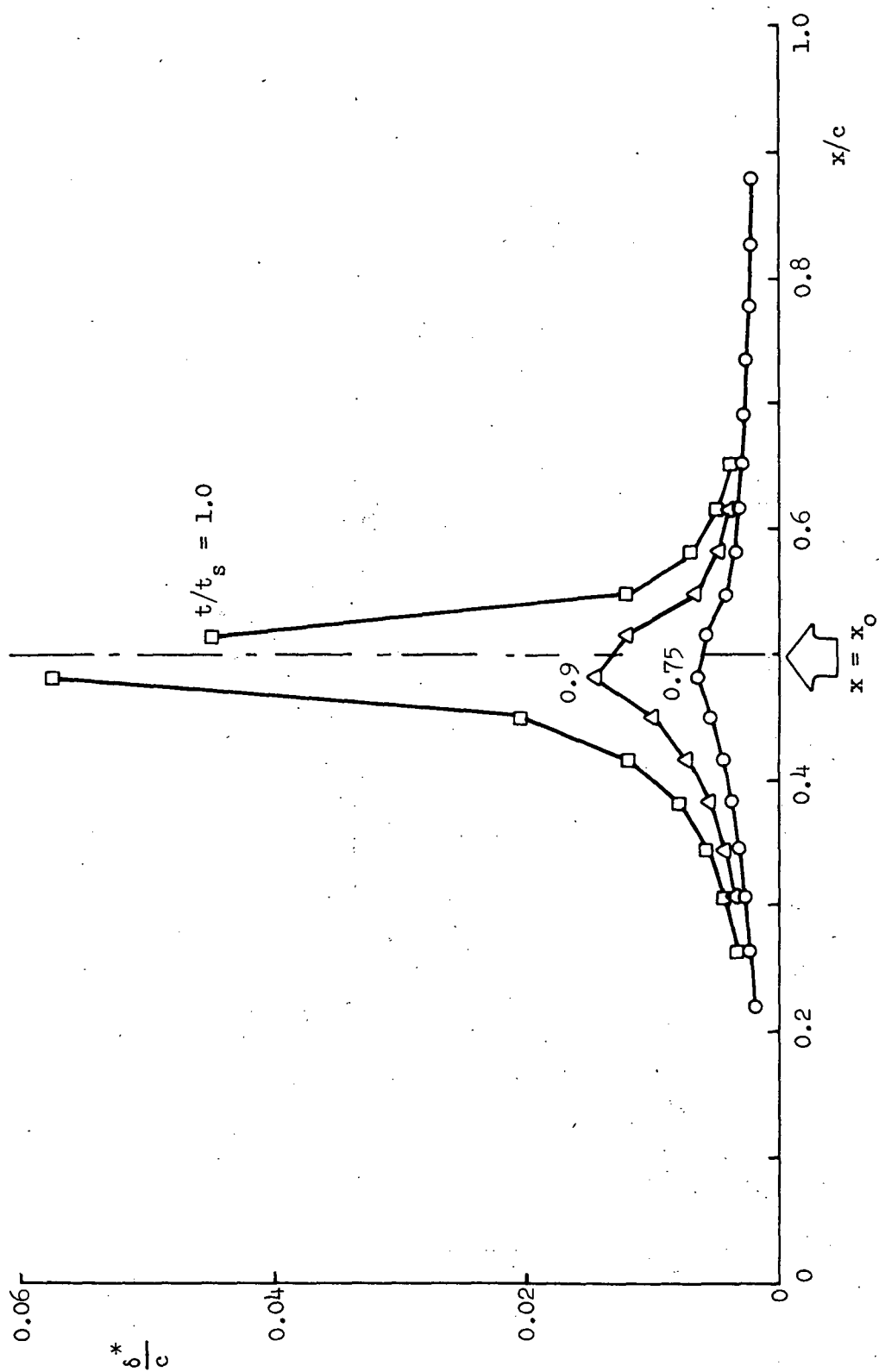
Figure 3. Displacement Thickness Distributions for Increasing Time $\left(c\omega/U_o = 10 \right)$

24
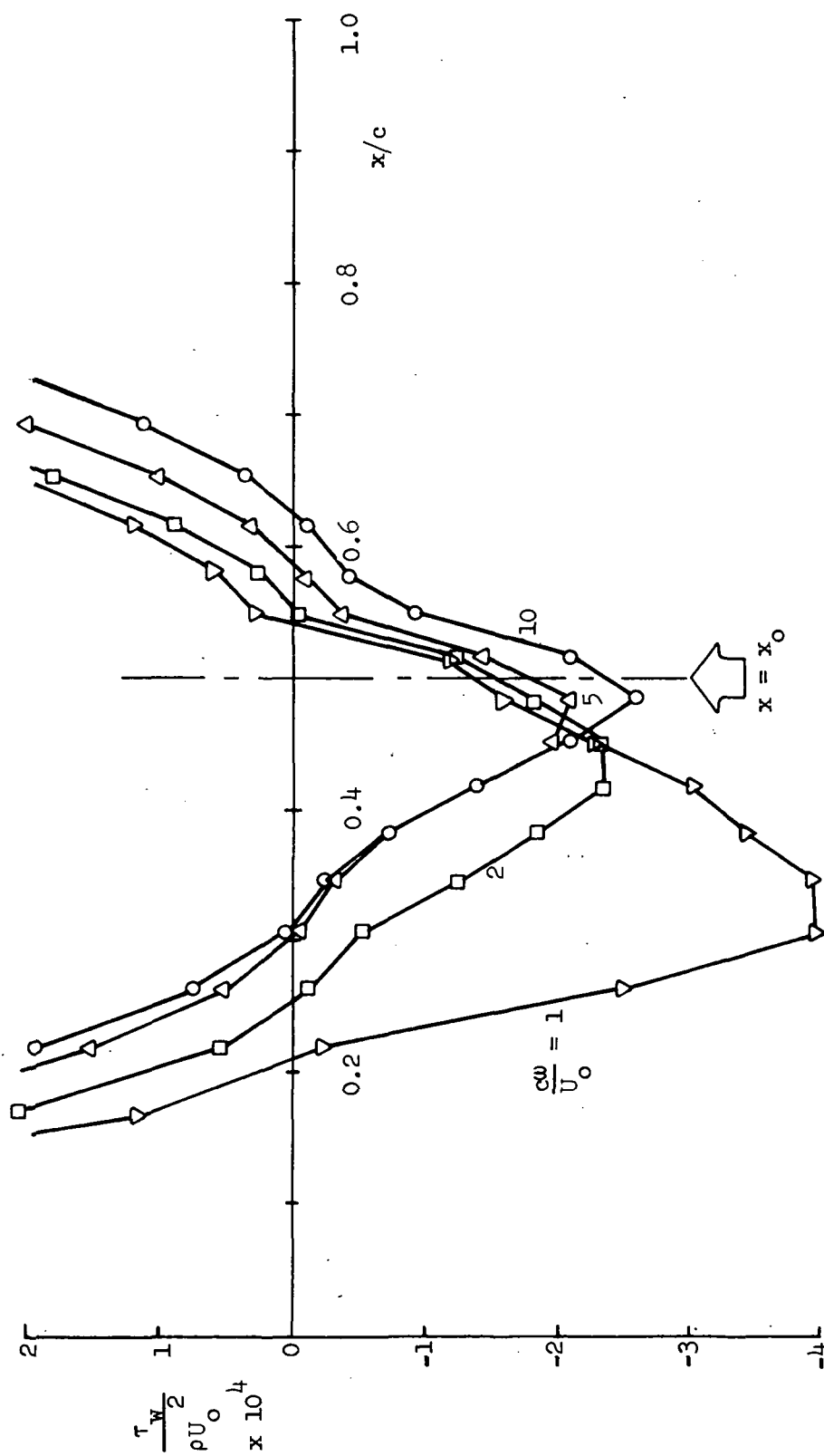
Figure 4. Wall Shear Stress Distributions for a Range of ω $\left(t = t_s \right)$
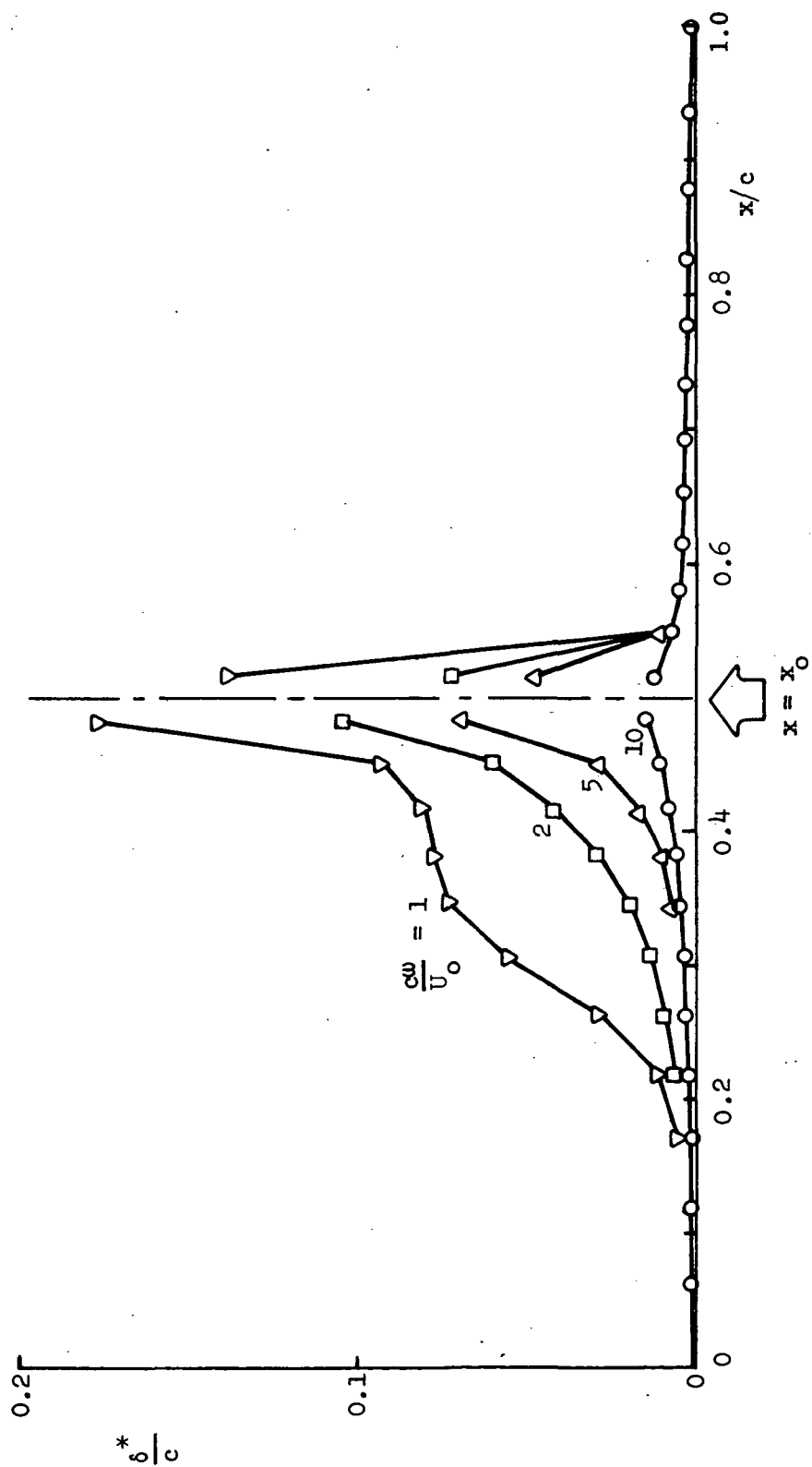
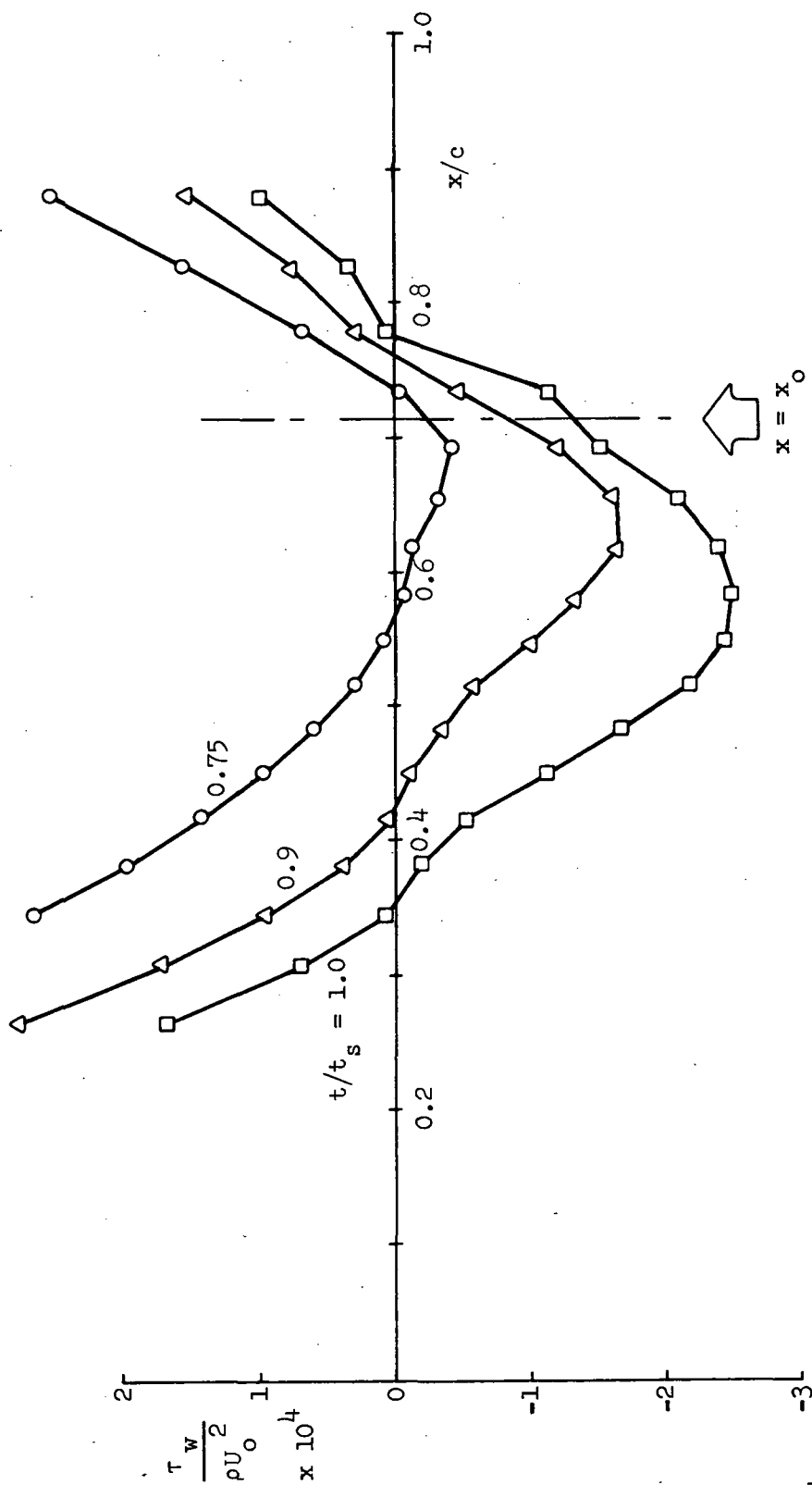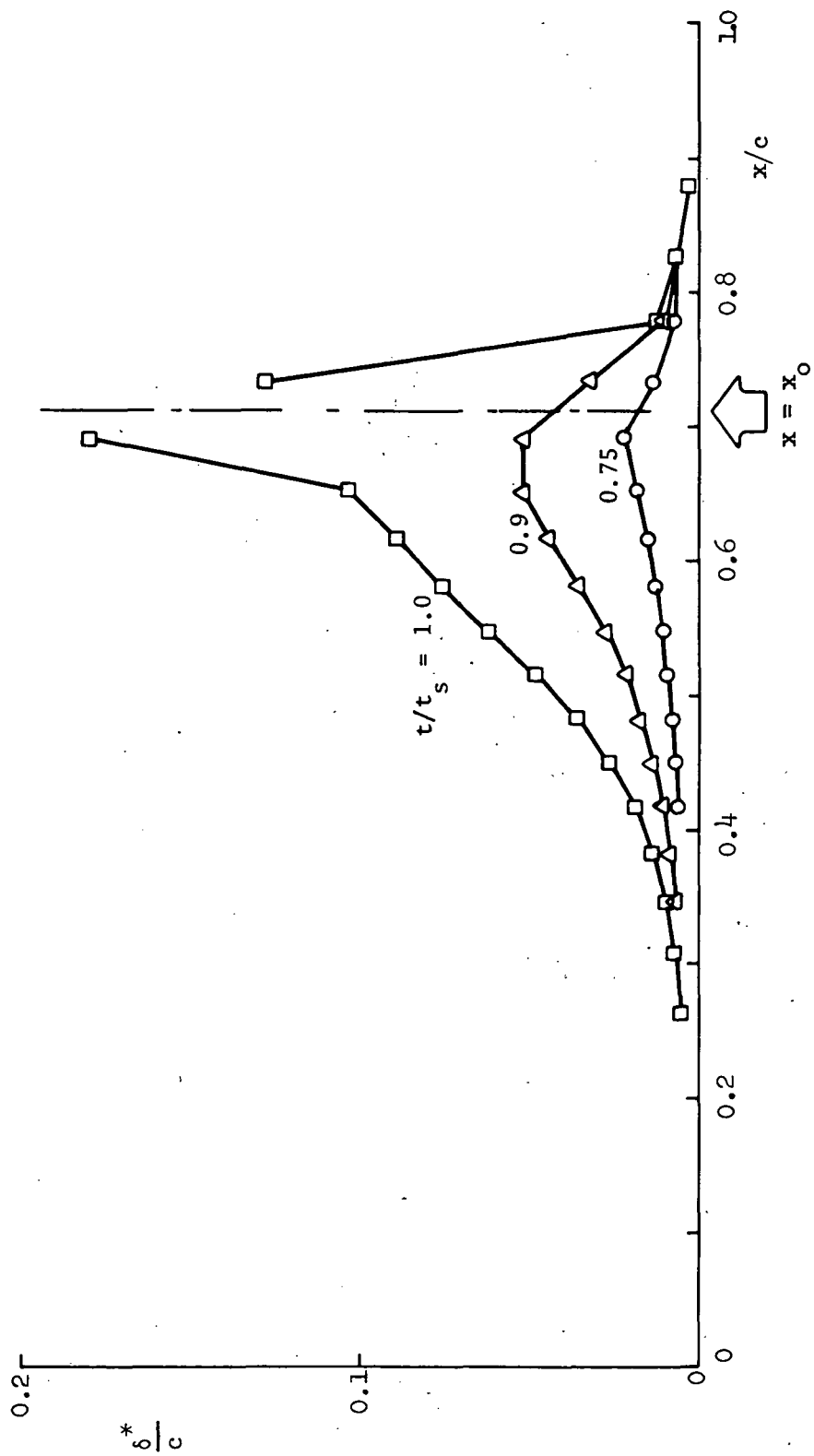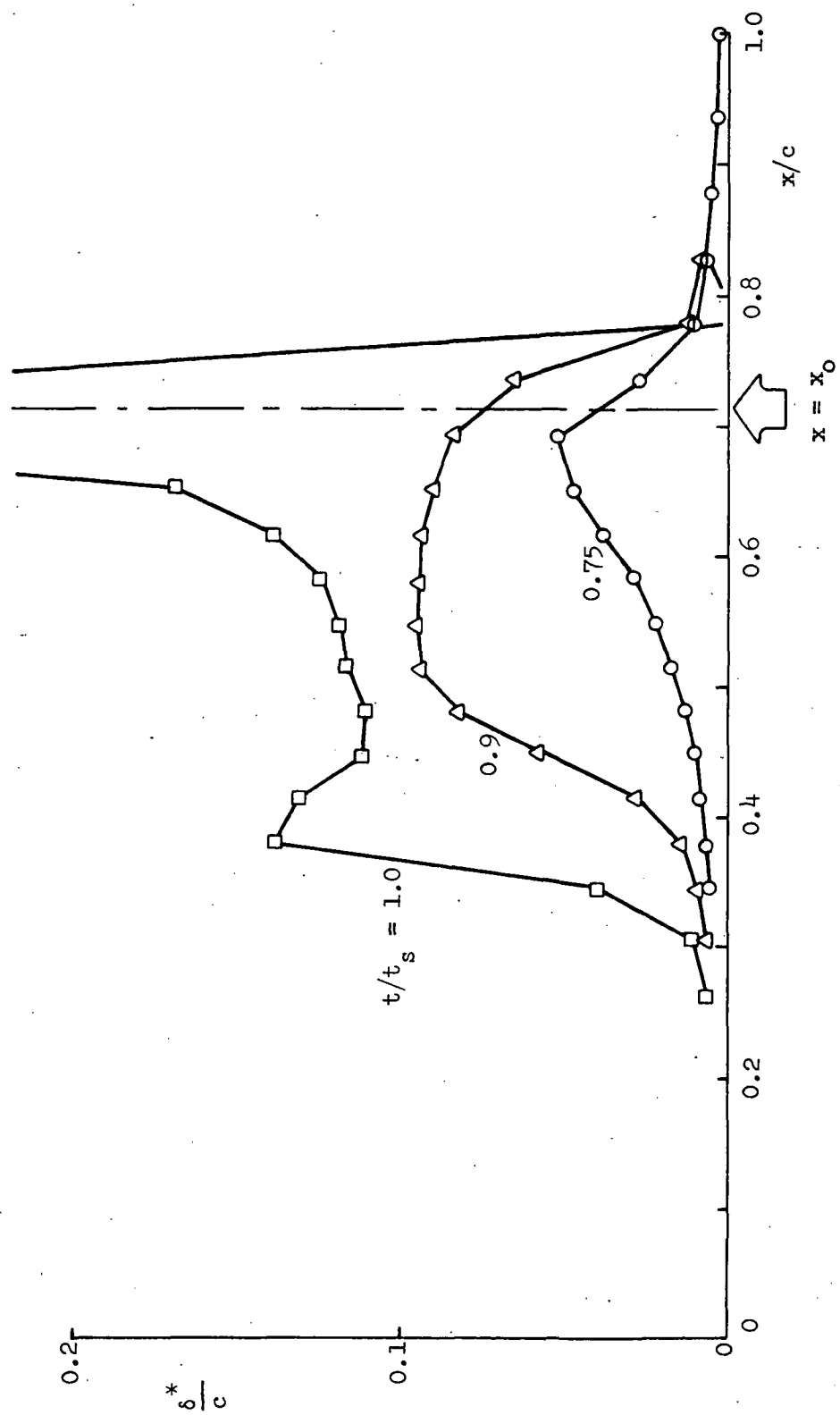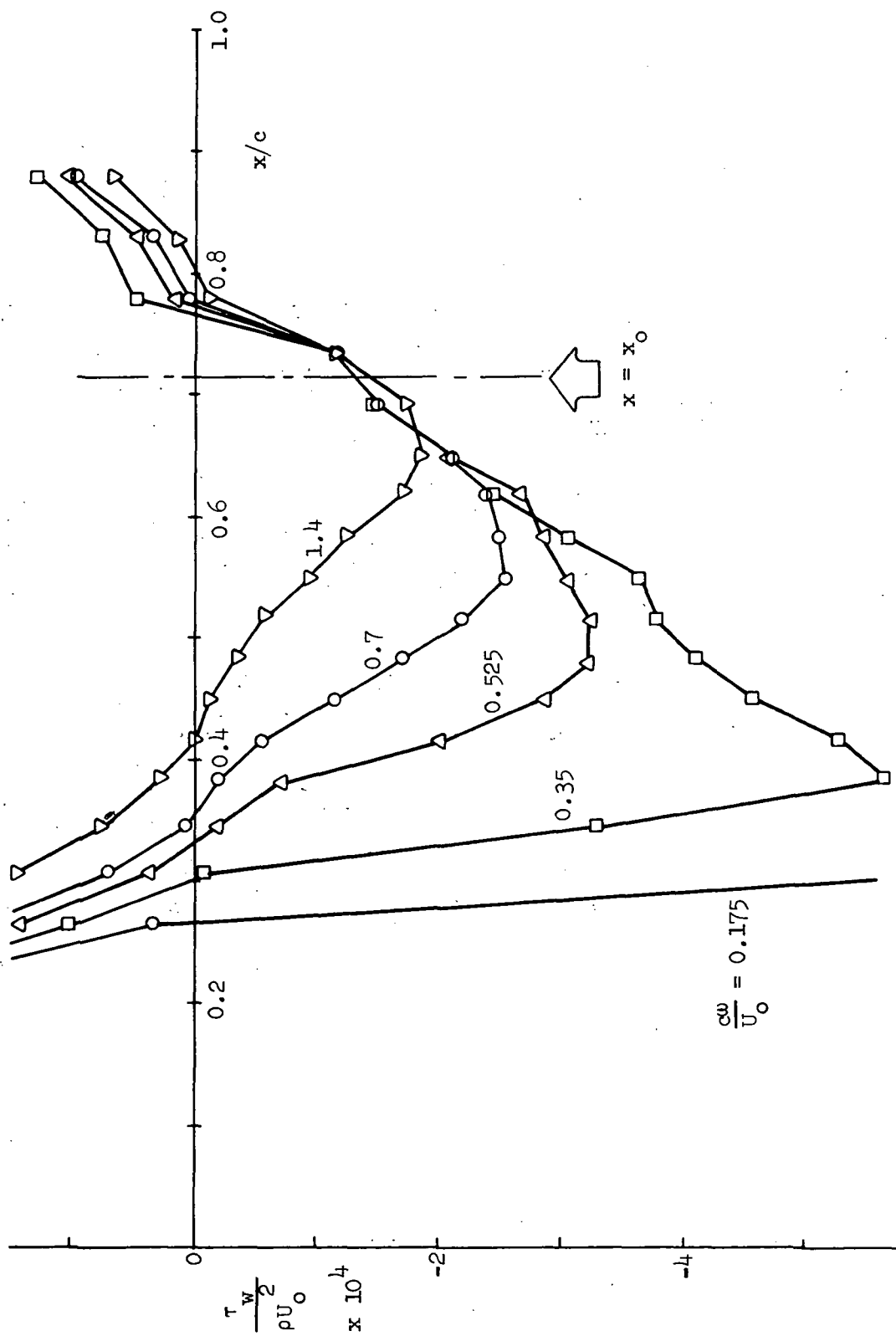Figure 5. Displacement Thickness Distributions for a Range of ω $\left(t = t_s\right)$

Figure 6. Wall Shear Stress Distributions for Increasing Time $\left(c\omega/U_o = 0.7 \right)$

27

Figure 7. Displacement Thickness Distributions for Increasing Time $\left(c\omega/U_o = 0.7\right)$
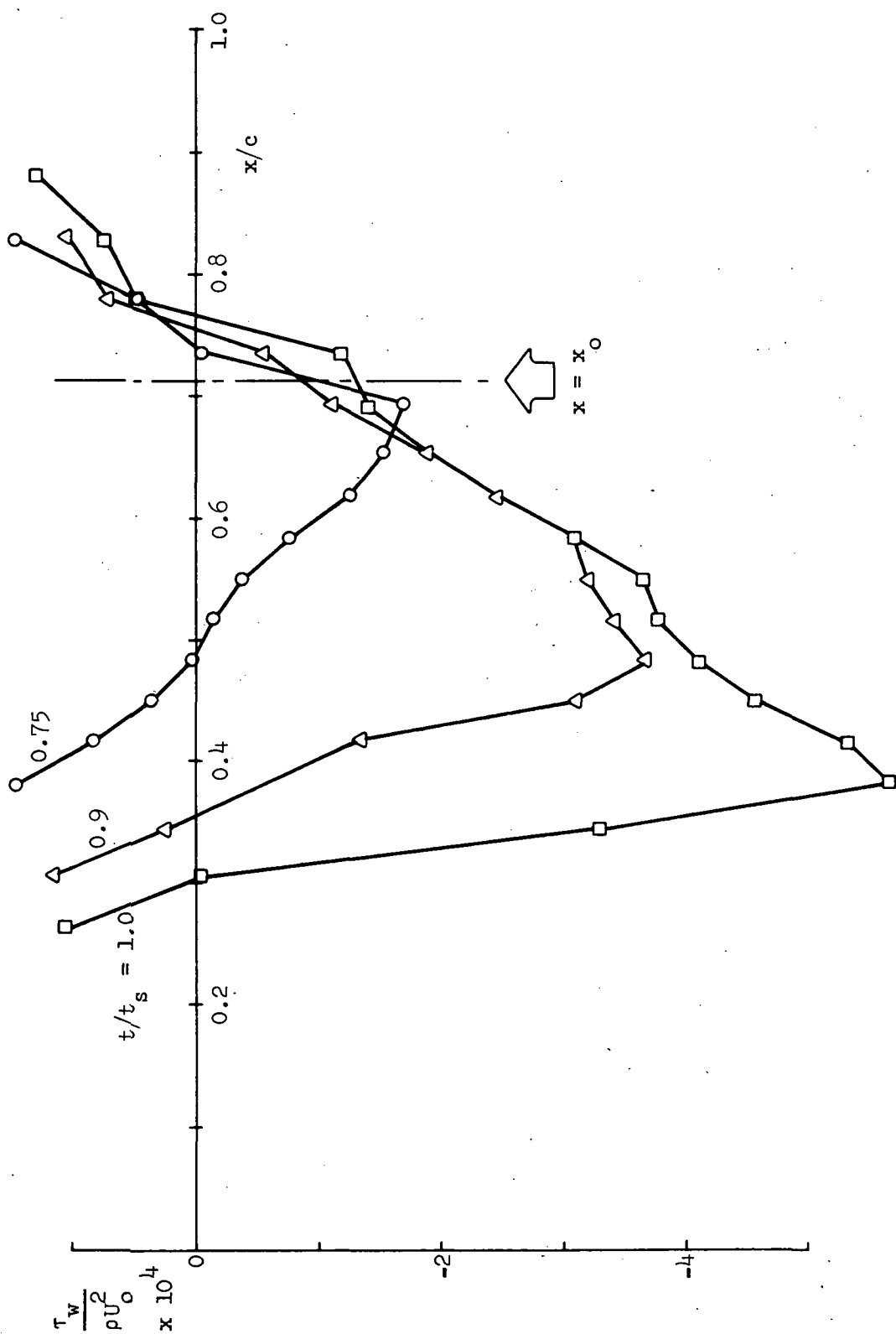
Figure 8. Wall Shear Stress Distributions for Increasing Time $\left(c\omega/U_o = 0.35 \right)$

29

Figure 9. Displacement Thickness Distributions for Increasing Time $\left(\dfrac{c\omega}{U_o} = 0.35 \right)$
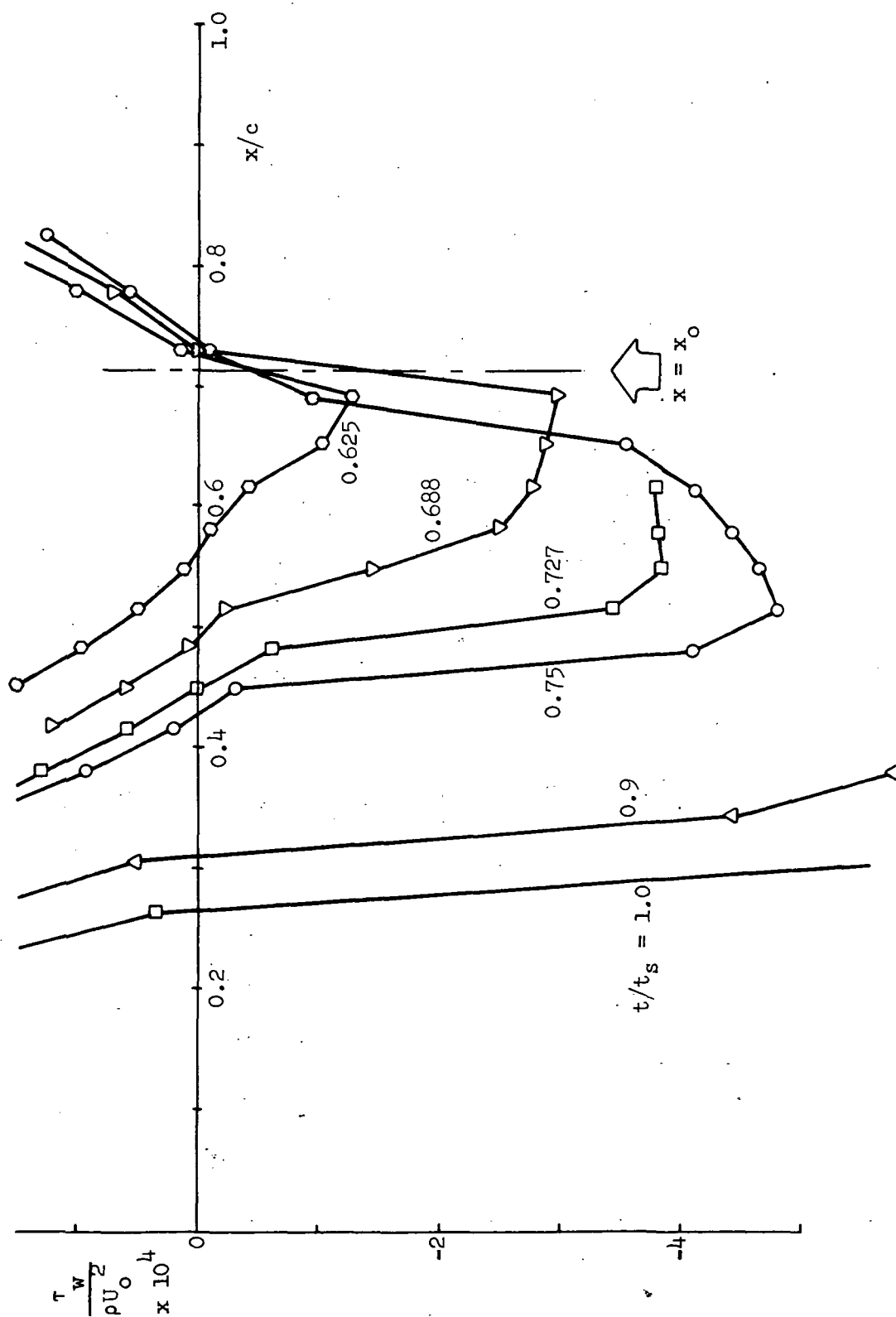
Figure 10. Wall Shear Stress Distributions for Increasing Time $\left(c\omega/U_o = 0.175\right)$

31

Figure 11. Displacement Thickness Distributions for Increasing Time $\left(\frac{cw}{U_o} = 0.175 \right)$

32

Figure 12. Wall Shear Stress Distributions for a Range of ω $\left(t = t_s \right)$

33
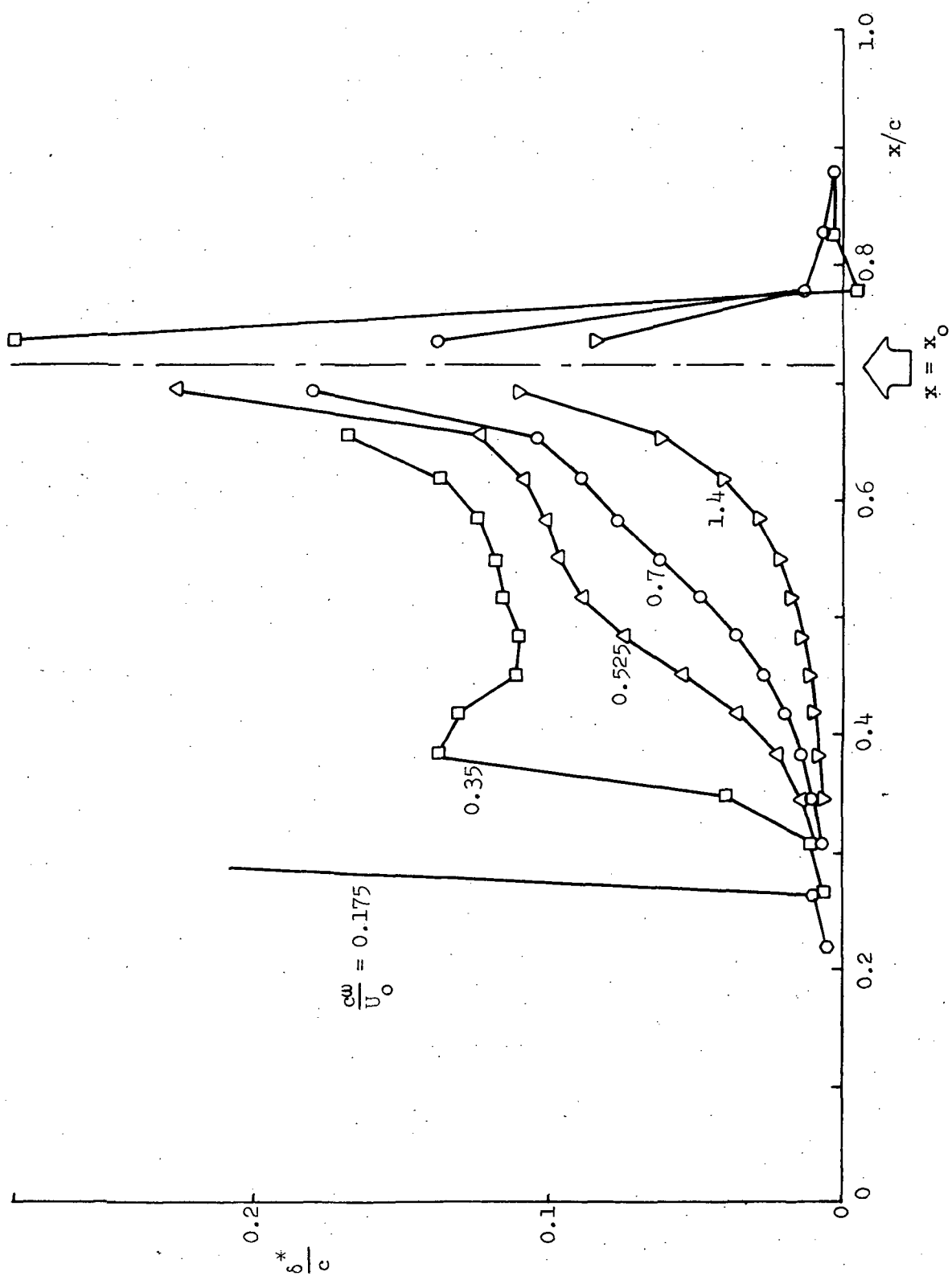
Figure 13. Displacement Thickness Distributions for a Range of ω

34
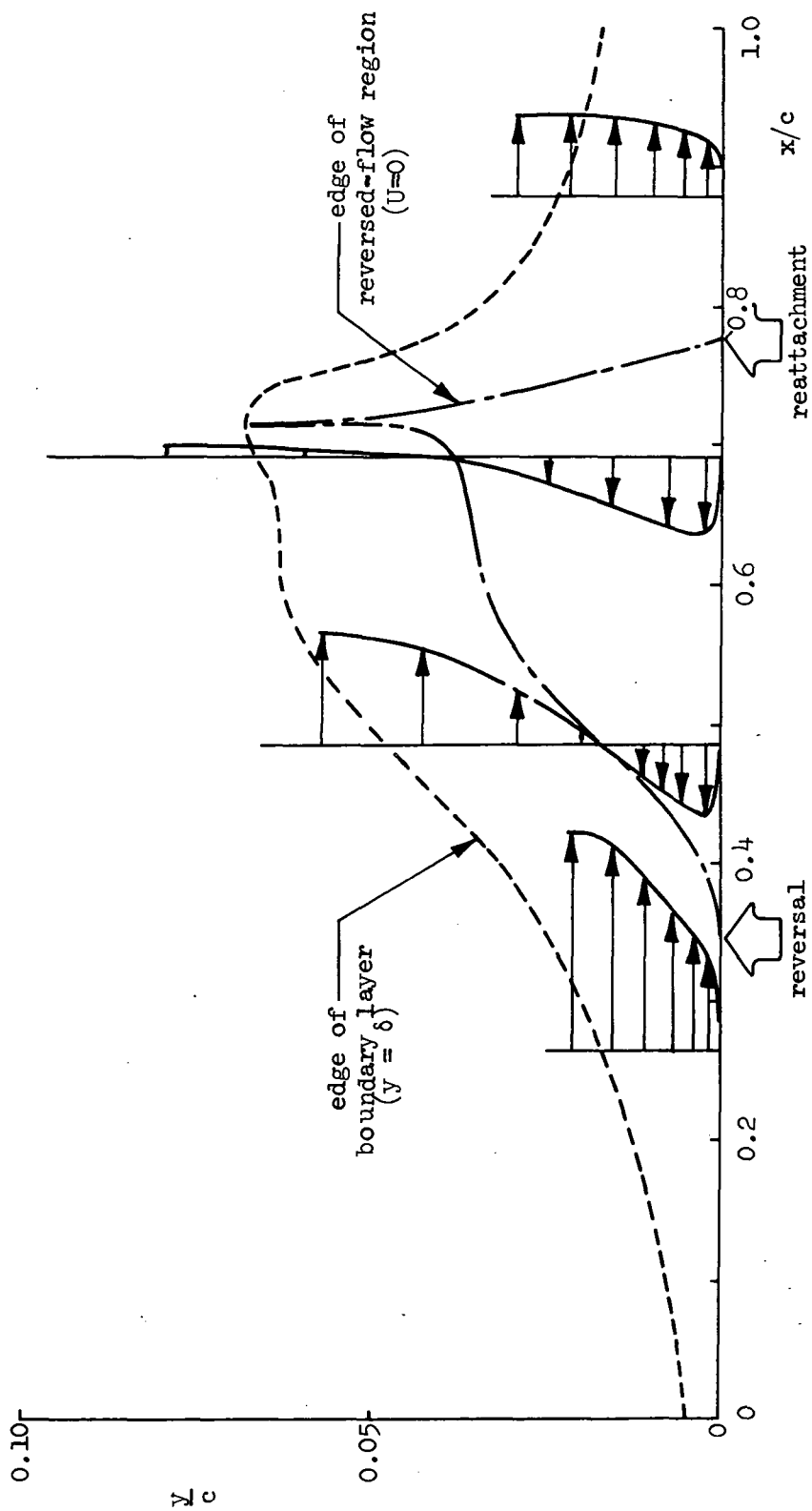
Figure 14. Gross Features of the Flow $\left(c\omega/U_o = 0.7,\ t = t_s\right)$
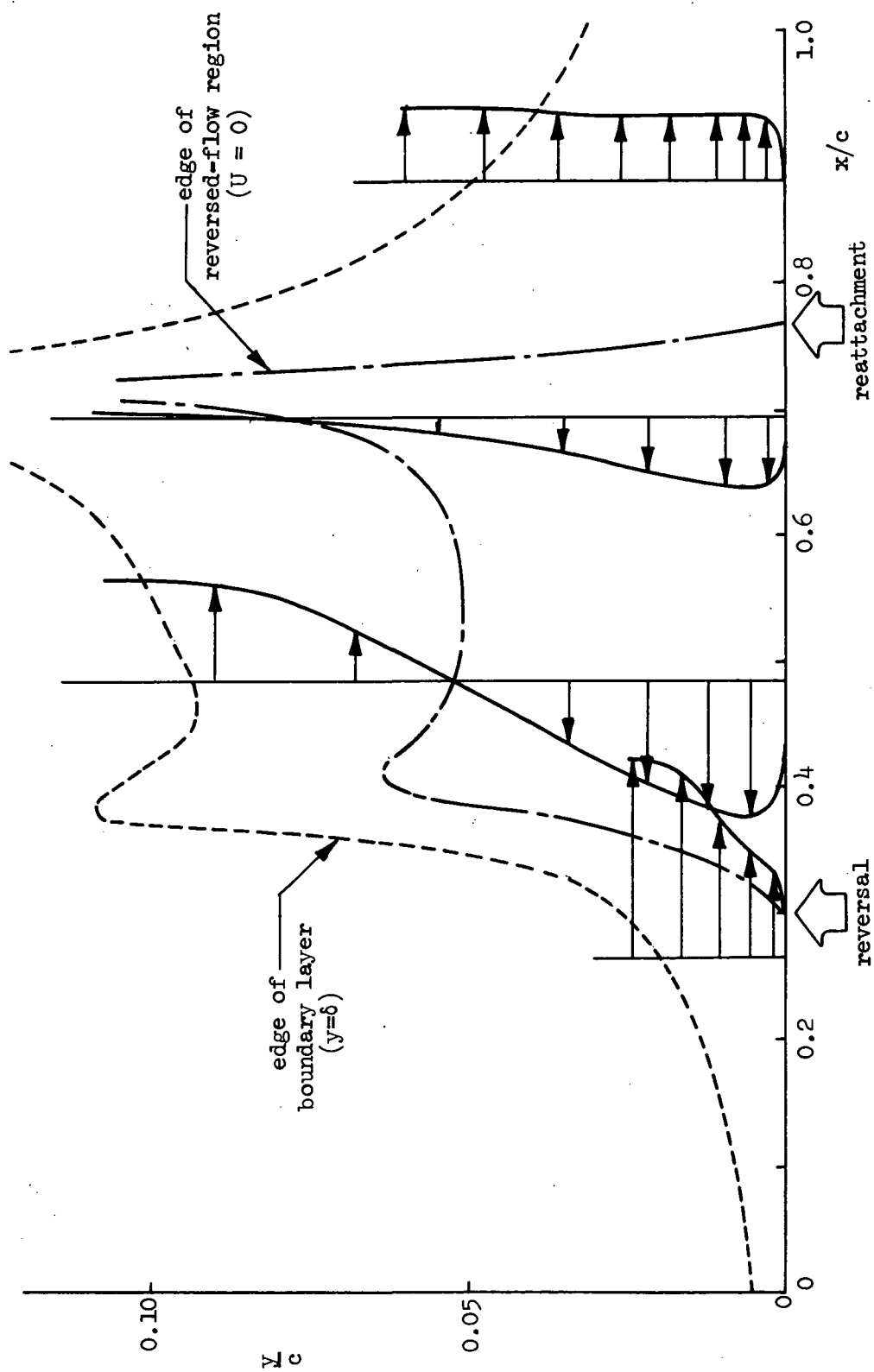
Figure 15. Gross Features of the Flow $\left(c\dot{\omega}/U_o = 0.35, \ t = t_s \right)$
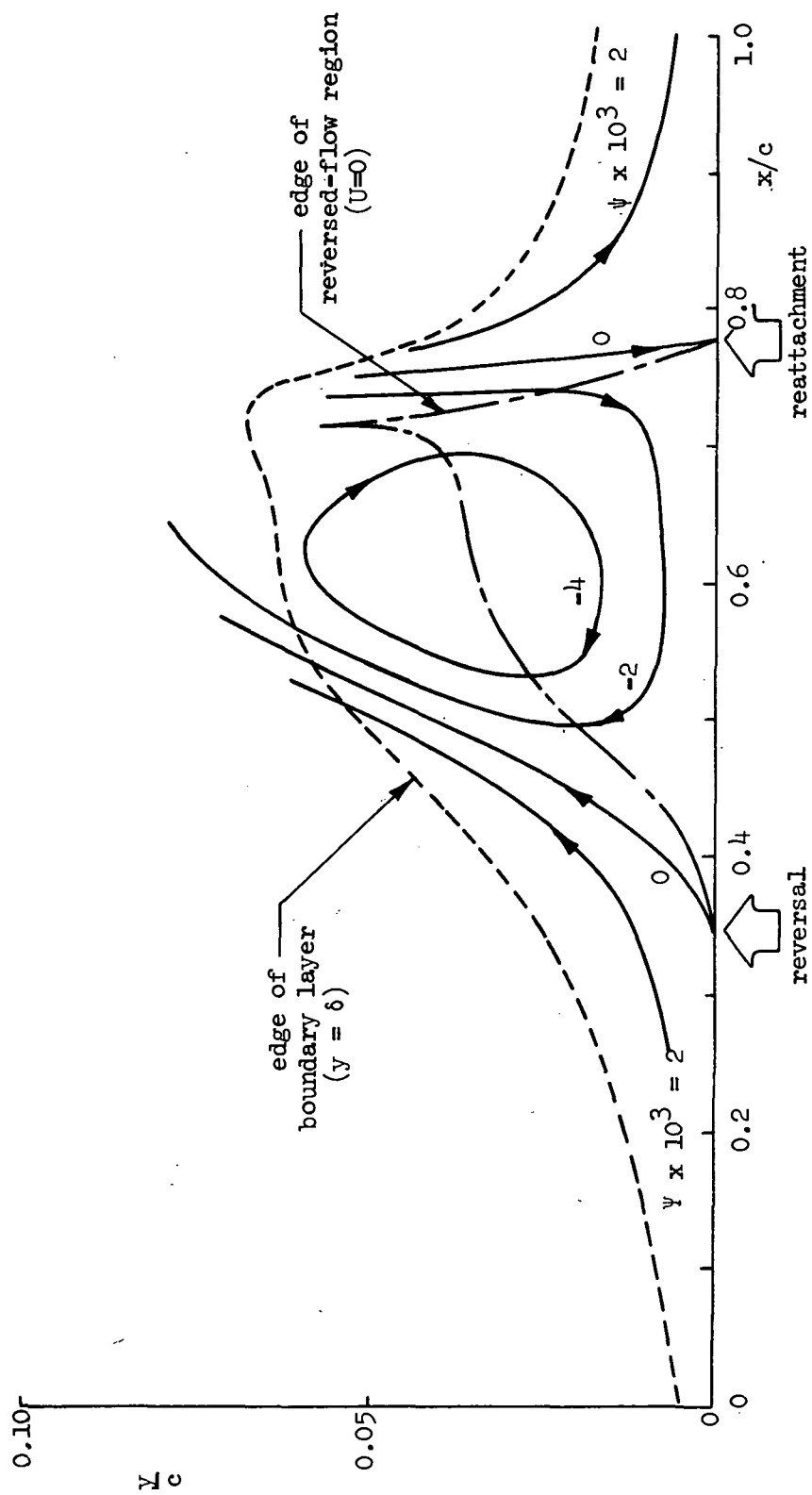
Figure 16. Streamline Patterns $\left(c\omega/U_o = 0.7, \ t = t_s \right)$
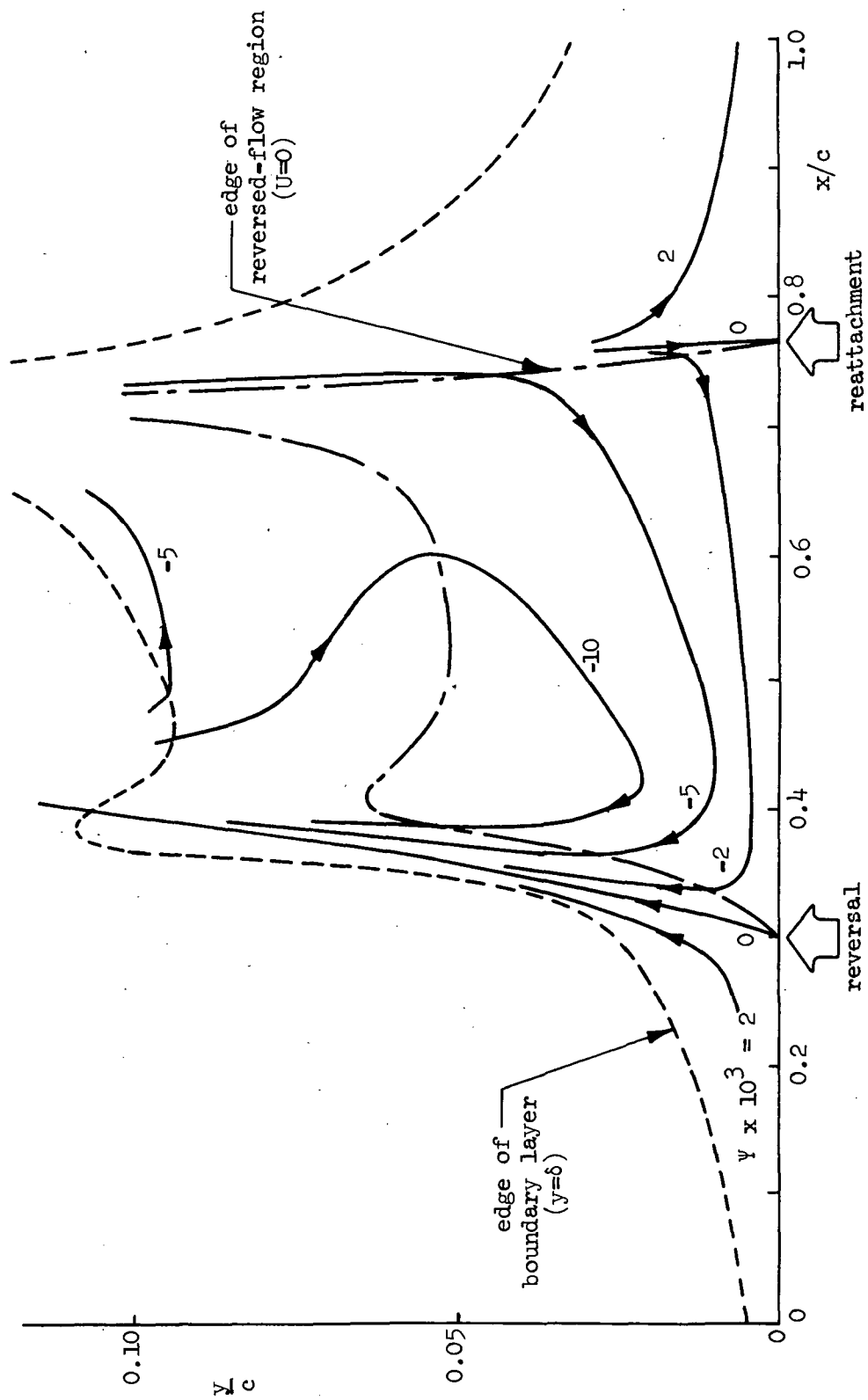
Figure 17. Streamline Patterns $\left(c\omega/U_o = 0.35, \; t = t_s \right)$
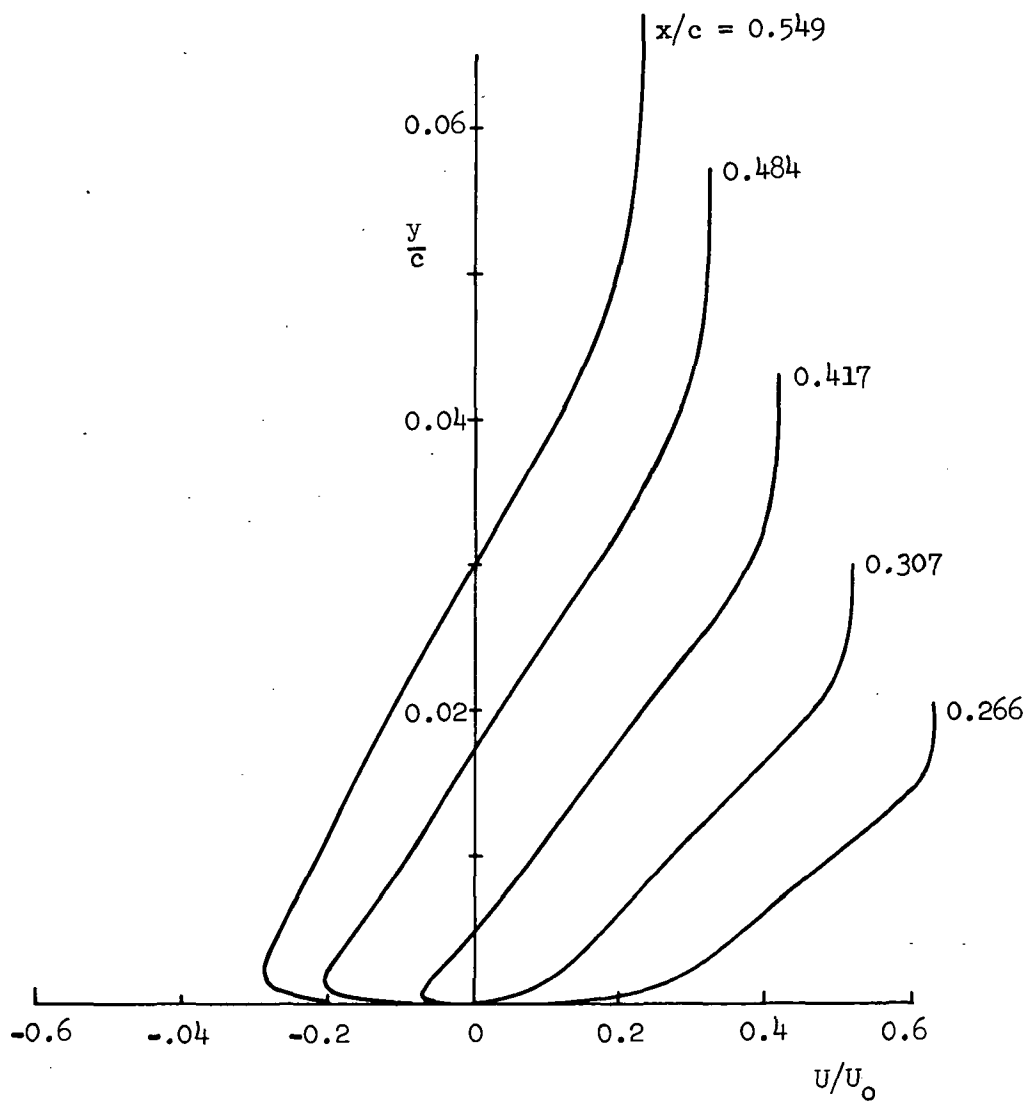
Figure 18. Velocity Profiles Near the Reversal Point $\left(c\omega/U_o = 0.7, \; t = t_s \right)$

Figure 19. Velocity Profiles Near the Reversal Point $\left(\alpha\omega/U_o = 0.35, \quad t = t_s\right)$
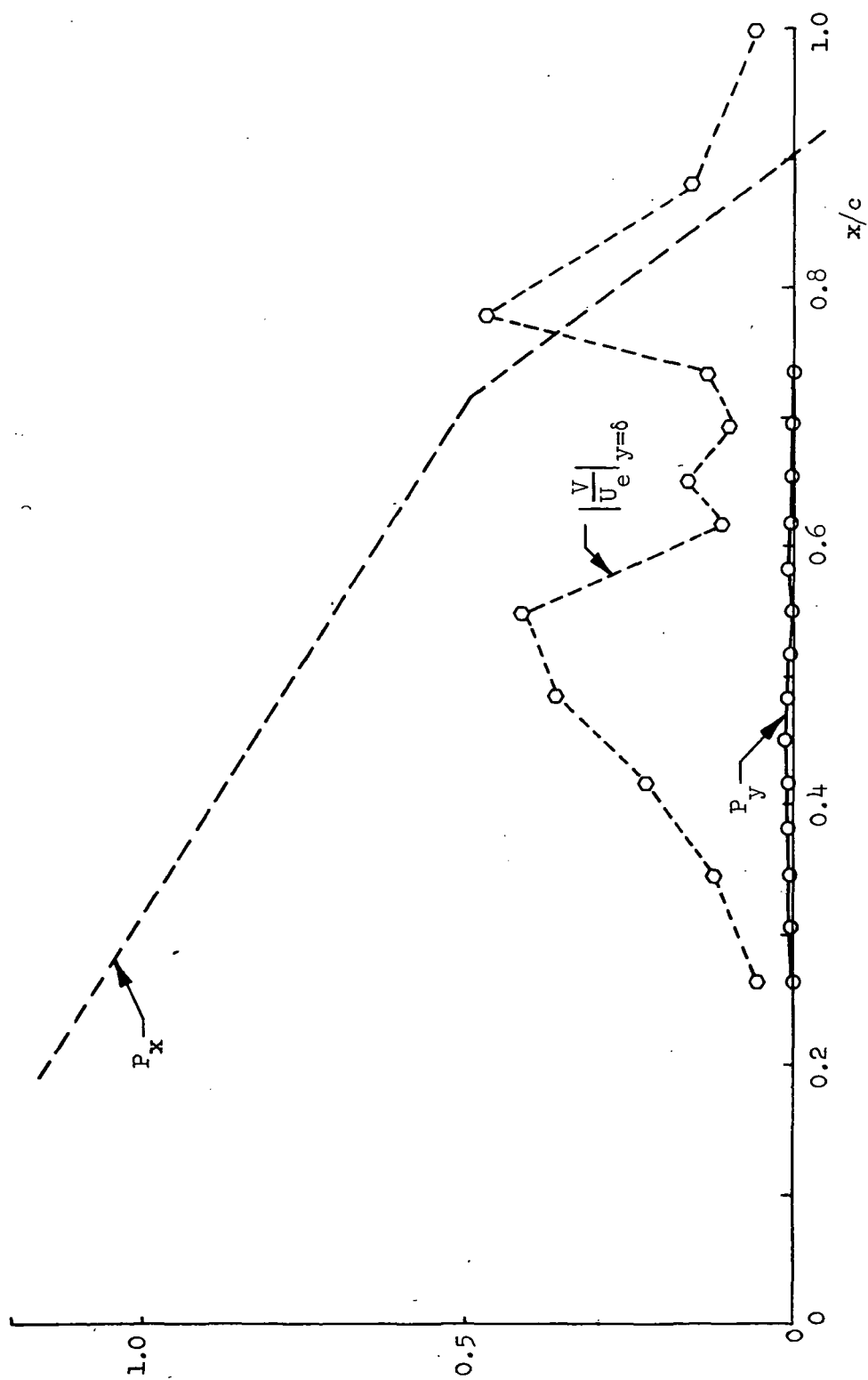
Figure 20. Test for Validity of the Boundary-Layer Approximations $\left(c\omega/U_o = 0.7, \; t = t_s \right)$
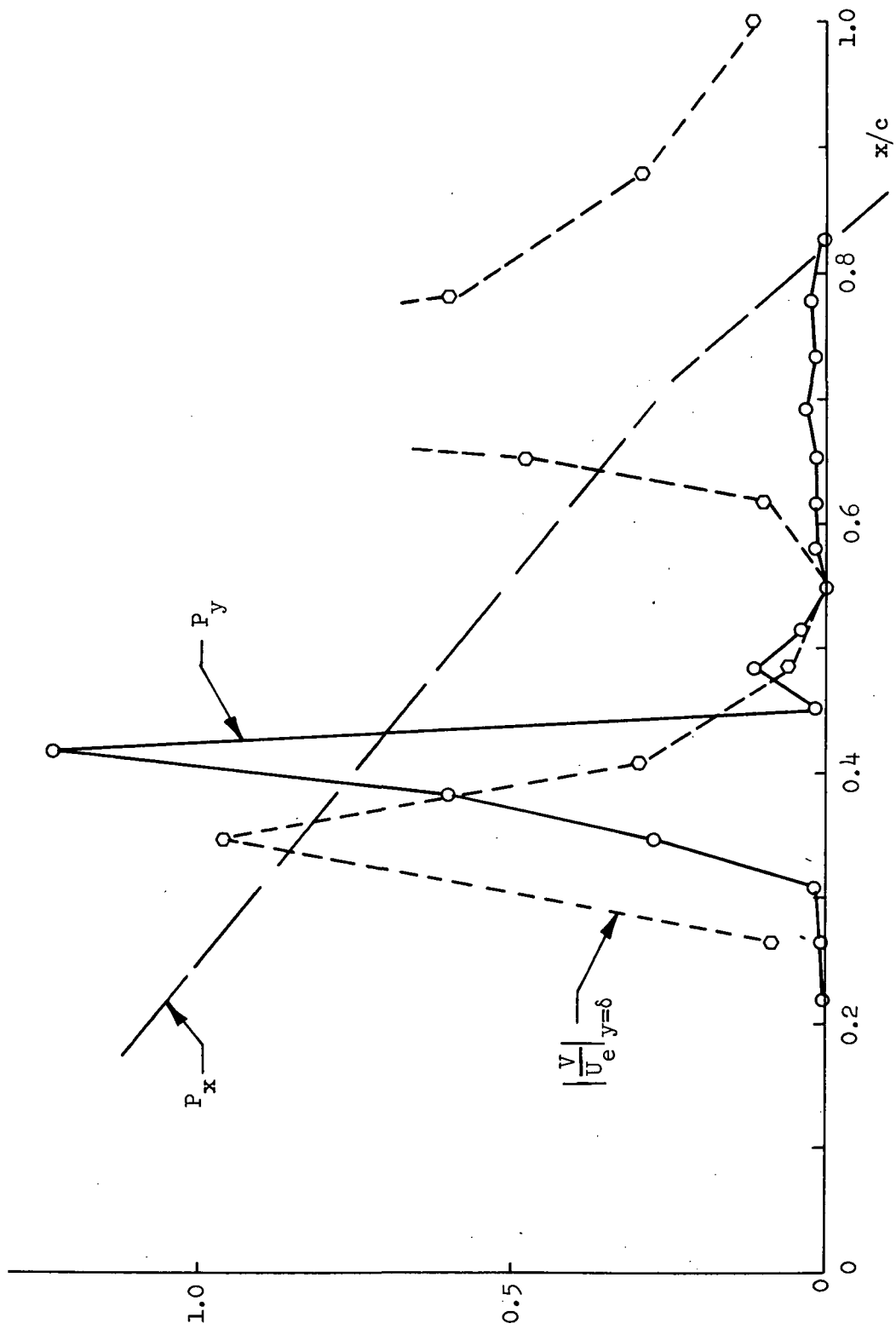
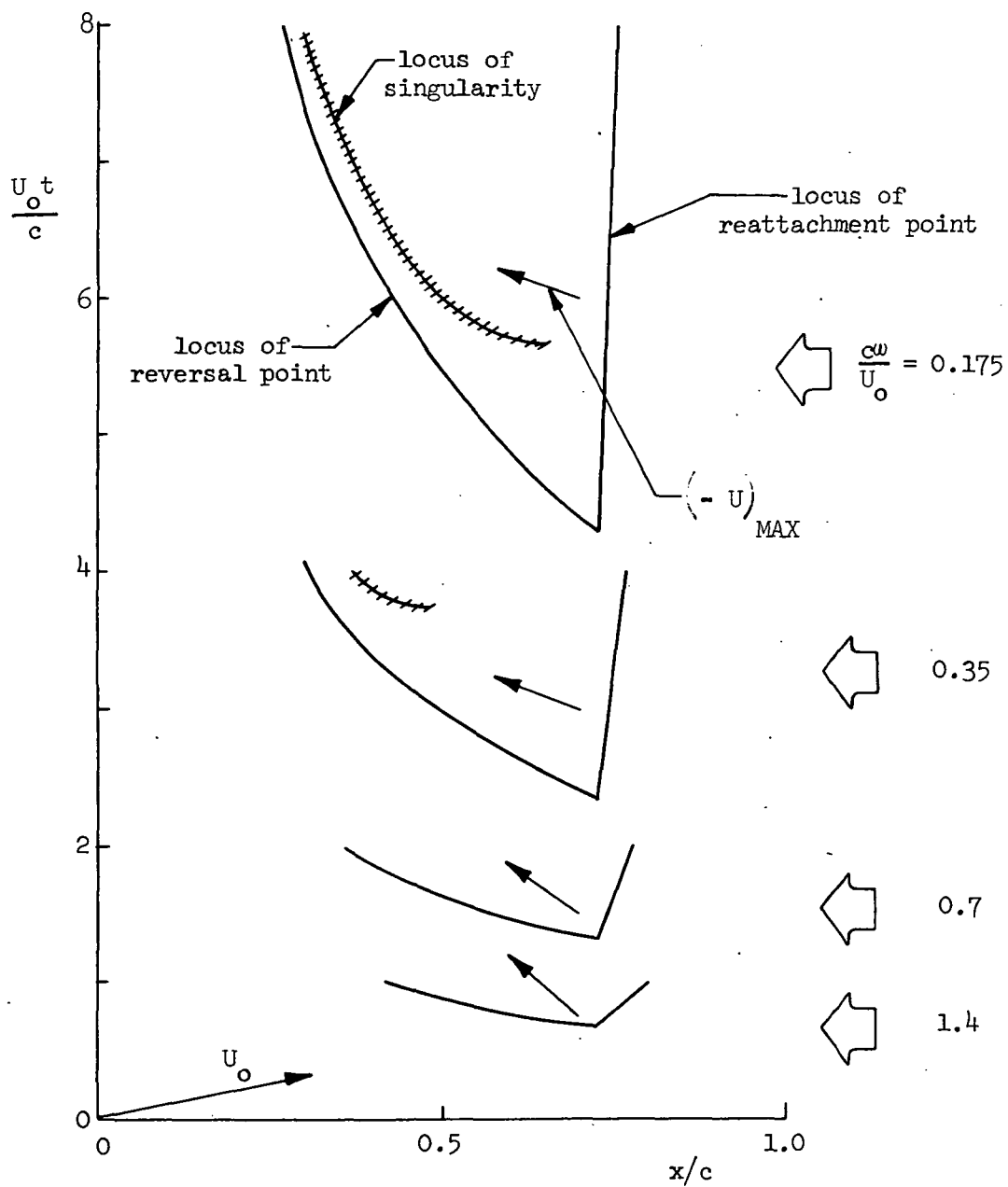Figure 21. Test for Validity of the Boundary-Layer Approximations $\left(\alpha w/U_o = 0.35, \ t = t_s \right)$

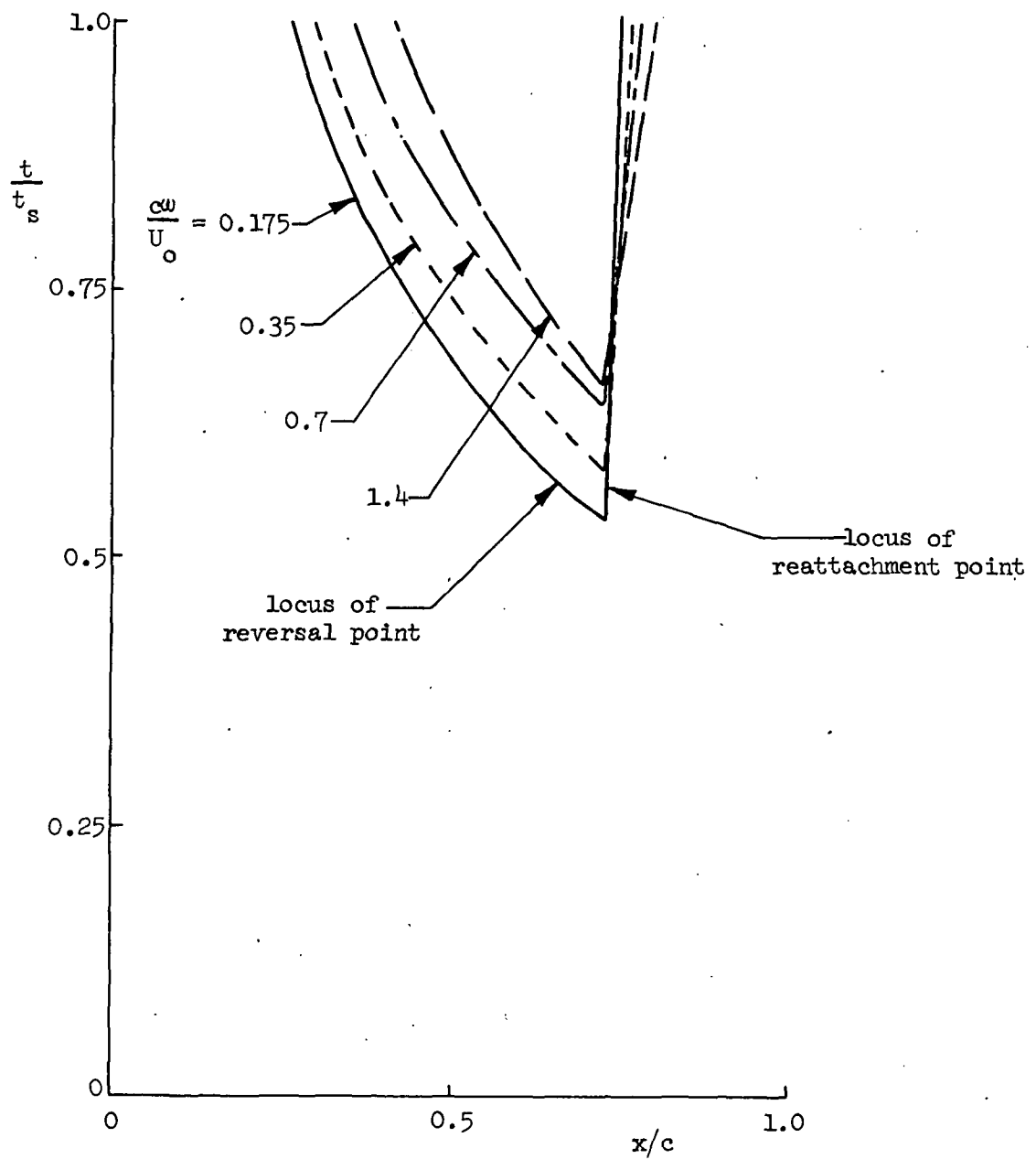Figure 22. Temporal Development of the Reversed-Flow Region for a Range of ω

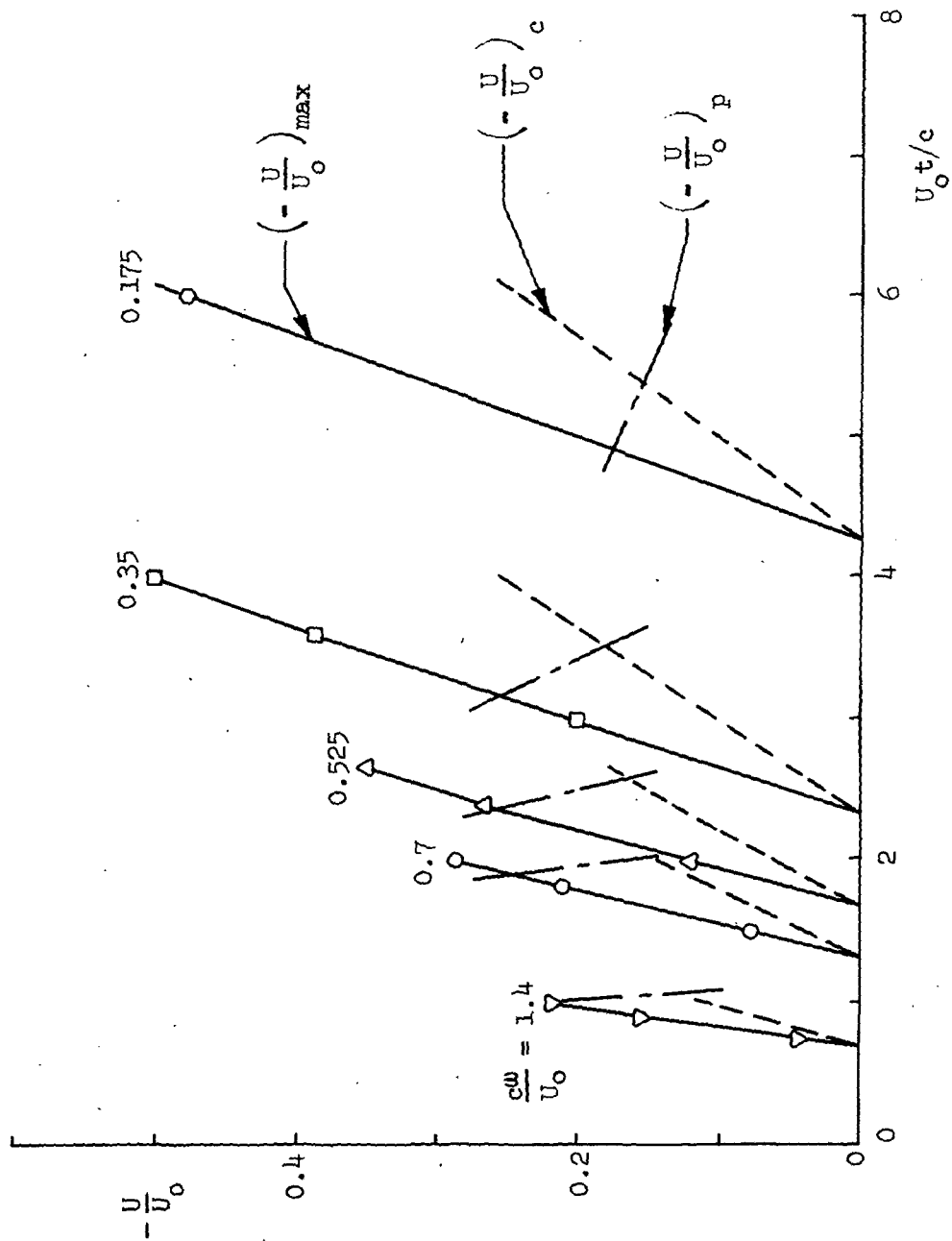Figure 23. Similarity of Development of the Reversed-Flow Region

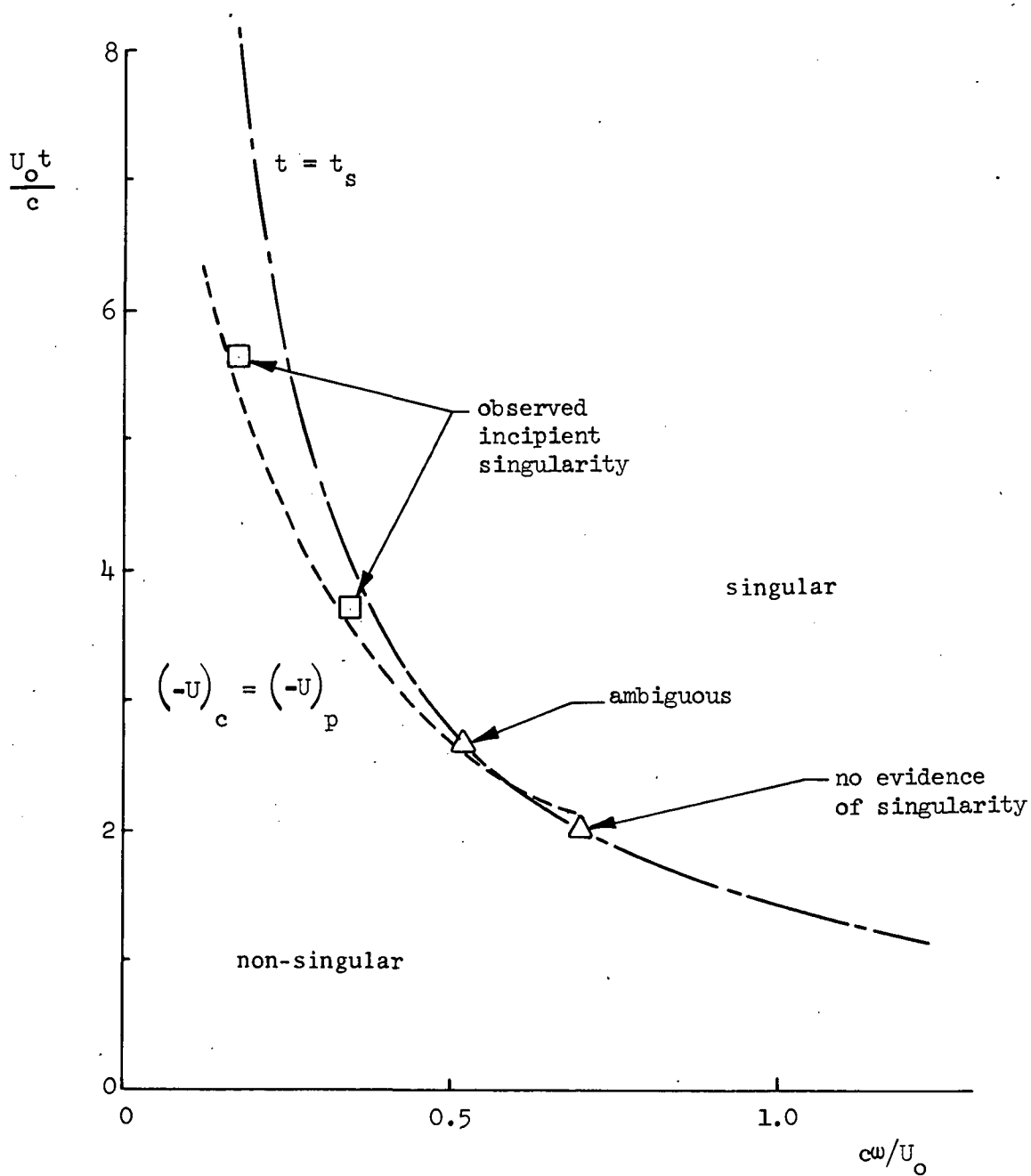Figure 24. Average Convection Velocity and Penetration Velocity.

Figure 25. Boundary of the Domain of Non-Singular Flow

"The aeronautical and space activities of the United States shall be conducted so as to contribute . . . to the expansion of human knowledge of phenomena in the atmosphere and space. The Administration shall provide for the widest practicable and appropriate dissemination of information concerning its activities and the results thereof."
—NATIONAL AERONAUTICS AND SPACE ACT OF 1958

NASA SCIENTIFIC AND TECHNICAL PUBLICATIONS

TECHNICAL REPORTS: Scientific and technical information considered important, complete, and a lasting contribution to existing knowledge.

TECHNICAL NOTES: Information less broad in scope but nevertheless of importance as a contribution to existing knowledge.

TECHNICAL MEMORANDUMS: Information receiving limited distribution because of preliminary data, security classification, or other reasons. Also includes conference proceedings with either limited or unlimited distribution.

CONTRACTOR REPORTS: Scientific and technical information generated under a NASA contract or grant and considered an important contribution to existing knowledge.

TECHNICAL TRANSLATIONS: Information published in a foreign language considered to merit NASA distribution in English.

SPECIAL PUBLICATIONS: Information derived from or of value to NASA activities. Publications include final reports of major projects, monographs, data compilations, handbooks, sourcebooks, and special bibliographies.

TECHNOLOGY UTILIZATION PUBLICATIONS: Information on technology used by NASA that may be of particular interest in commercial and other non-aerospace applications. Publications include Tech Briefs, Technology Utilization Reports and Technology Surveys.

Details on the availability of these publications may be obtained from:

SCIENTIFIC AND TECHNICAL INFORMATION OFFICE

NATIONAL AERONAUTICS AND SPACE ADMINISTRATION
Washington, D.C. 20546